Copyright Warning & Restrictions

The copyright law of the United States (Title 17, United States Code) governs the making of photocopies or other reproductions of copyrighted material.

Under certain conditions specified in the law, libraries and archives are authorized to furnish a photocopy or other reproduction. One of these specified conditions is that the photocopy or reproduction is not to be "used for any purpose other than private study, scholarship, or research." If a, user makes a request for, or later uses, a photocopy or reproduction for purposes in excess of "fair use" that user may be liable for copyright infringement,

This institution reserves the right to refuse to accept a copying order if, in its judgment, fulfillment of the order would involve violation of copyright law.

Please Note: The author retains the copyright while the New Jersey Institute of Technology reserves the right to distribute this thesis or dissertation

Printing note: If you do not wish to print this page, then select "Pages from: first page # to: last page #" on the print dialog screen

ABSTRACT

NMR COMPUTER SIMULATION OF GLASSY AND POWDERED SAMPLES: APPLICATION TO STUDIES OF SODIUM BOROVANADATE GLASSES

by
Xian-Quan Zhang

A computer program is devised to simulate the nuclear magnetic resonance (NMR) spectra observed in powdered and glassy samples in the presence of both nuclear quadrupole and anisotropic chemical shift interactions. This method is performed for the central transition of NMR spectra of nuclei with half-integral spin I. Typical theoretical behavior of the powder pattern is discussed and the "noise" and "error" in the simulated spectra are analyzed. The computer simulation method is applied to the studies of ^{11}B NMR spectra of the sodium borovanadate glass system for which a structural model is presented in the range for which glasses can be made. The model predictions are in good agreement with the experimental data obtained by the ^{11}B NMR computer simulation technique.

NMR COMPUTER SIMULATION OF GLASSY AND POWDERED SAMPLES: APPLICATION TO STUDIES OF SODIUM BOROVANADATE GLASSES

by
Xian-Quan Zhang

A Thesis
Submitted to the Faculty of
New Jersey Institute of Technology
in Partial Fulfillment of the Requirements for the Degree of
Master of Science in Applied Physics

Department of Physics

May 1994

APPROVAL PAGE

NMR COMPUTER SIMULATION OF GLASSY AND POWDERED SAMPLES: APPLICATION TO STUDIES OF SODIUM BOROVANADATE GLASSES

Xian-Quan Zhang

Dr. Onofrio L. Russo, Thesis Advisor — Date
Associate Professor of Physics
New Jersey Institute of Technology

Dr. Leon Buteau, Committee Member — Date
Chairman and Professor of Physics
New Jersey Institute of Technology

Dr. Nuggegalli M. Ravindra, Committee Member — Date
Associate Professor of Physics
New Jersey Institute of Technology

BIOGRAPHICAL SKETCH

Author: Xian-Quan Zhang

Degree: Master of Science in Applied Physics

Date: May 1994

Undergraduate and Graduate Education:

- Master of Science in Applied Physics,
  New Jersey Institute of Technology, Newark, NJ, 1994
- Master of Science in Radio-frequency Spectroscopy,
  East China Normal University, Shanghai, P. R. China
- Bachelor of Science in Physics,
  East China Normal University, Shanghai, P. R. China

Major: Applied Physics

This thesis is dedicated to
my wife, Mrs. Ping Zuo Zhang, and my son, Tao-Yuan Zhang

ACKNOWLEDGMENT

The author wishes to express his sincere gratitude to his advisor, Dr. Onofrio L. Russo, for his guidance, friendship, and moral support throughout this research.

The author also wishes to thank to Dr. Leon Buteau and Dr. Nuggegalli M. Ravindra for serving as members of the committee.

TABLE OF CONTENTS

LIST OF TABLES

LIST OF FIGURES

CHAPTER 1

INTRODUCTION

The structural and dynamical properties of many kinds of solid materials can be obtained from nuclear magnetic resonance (NMR). The NMR spectra of many solids are affected by both nuclear quadrupole interactions and chemical shift effects. When a single crystal is under study, it is a fairly straightforward process to separate the two effects. However, if only a powdered sample or a glass is available it is a rather difficult process to obtain the relevant quadrupolar and chemical shift parameters from the resulting NMR spectra. Information from NMR studies of powdered or glassy materials has been limited because of a shortage of appropriate computational techniques from which the relevant theoretical parameters of the derivative-like spectra can be obtained. Fig.5c shows an example of the derivative-like spectrum for the corresponding absorption function.

A computer program is devised to simulate the NMR spectra occuring in powdered and glassy samples. The theoretical behaviors (such as the locations of shoulders and singularities) in these NMR spectra are discussed. The powder patterns are calculated for the central transition of NMR of nuclei with half-integral spin I in the presence of nuclear quadrupolar and the anisotropic chemical shift interactions.The powder pattern is convoluted with a Gaussian function that simulates the effects of dipolar interaction broadening, and finally, the derivative of this result yields the function shape which is compared with the actual experimental trace.

With the aid of the computer simulation method, we have studied ^{11}B NMR of the ternary glass system of sodium borovanadate. In addition to the determinations of the parameters of the quadrupolar, anisotropic chemical shift

and the electrical field asymmetry parameter, values are obtained as a function of $R=mol\%Na_2O/mol\%B_2O_3$ (for each of the different values of $K=mol\%V_2O_5/mol\%B_2O_3$) for the fractions of boron in the following: BO_4 units (N_4) with four tetrahedral coordinated oxygens, symmetric BO_{3S} units (N_{3S}) with either zero or three non-bridging oxygens (NBO's), and asymmetrical BO_{3A} units (N_{3A}) with one and two NBO's. A structural model is presented for the glass system within the glass-formable region. The model predictions are in good agreement with the experimental data obtained by computer simulation techniques.

CHAPTER 2

NMR CONDITIONS AND POWDER PATTERNS

When the nucleus with spin I is placed in a constant magnetic field H_0, the total interaction Hamiltonian is

$$\mathcal{H}_{total}=\mathcal{H}_z+\mathcal{H}_{in} \tag{1}$$

where $\mathcal{H}_z$ is Zeeman interaction of nuclei with an applied constant magnetic field. $\mathcal{H}_{in}$ includes the nuclear quadrupole interaction, chemical shift effect and the dipole-dipole interaction [1,2,3]

$$\mathcal{H}_z=-\gamma\hbar\vec{I}\cdot\vec{H}_0 \tag{2}$$

$$\mathcal{H}_{in}=\mathcal{H}_Q+\mathcal{H}_{cs}+\mathcal{H}_{D\text{-}D} \tag{3}$$

where γ is the gyromagnetic ratio, and I is the nuclear spin operator.

For a nucleus which is entirely isolated from its surroundings ("bare nucleus"), only $\mathcal{H}_z$ is available and the resonance condition is given by

$$\nu_0=\frac{\lambda H_0}{2\pi} \tag{4}$$

When placed in a solid, the nucleus also experiences several internal interactions which are nuclear quadrupole interactions, chemical shift effects and dipole-dipole interactions. These interactions will cause an additional shift of the resonance frequency location away from that of its "bare nucleus" position. The amount of shift will generally depend on the orientation of the nuclear environment relative to the applied magnetic field. In a single crystal, the resonance condition can be written generally as

$$\nu=\nu(\mu,\phi) \qquad (\mu=\cos\theta) \tag{5}$$

where θ and ϕ are polar angles between axes fixed in the crystal and the direction of the applied magnetic field H_0. When the crystal is rotated (θ and ϕ are varied), the location of the resonance frequency will shift.

For a glassy or powdered sample, all nuclear spin I "sites" will exist with random orientations relative to H_0. In order to obtain the resonance spectrum, the resonance condition must be averaged over all possible nuclear site orientations. Assuming an individual "site" to have equal probability of being oriented in any element of solid angle with respect to the direction of field H_0, the absorption at frequency ν in the interval $d\nu$ is given by [2]

$$P(\nu)d\nu = \frac{1}{4\pi}\int_{\nu}^{\nu+d\nu} I(\Omega)d\Omega(\nu') \qquad (6)$$

where $d\Omega(\nu)$ is an element of solid angle ($d\Omega = d\mu \cdot d\phi$) and $I(\Omega)$ is the probability for transition from initial state to final state [1].

$$I(\Omega) \propto |\langle m,I|\mathcal{H}'|I,m-1\rangle|^2 \propto I(I+1)-m(m-1)$$

where $\mathcal{H}'$ is the time dependent perturbation due to the rf field, $H_1(t)$, which causes the state transition. So, transition probabilities $I(\Omega)$ are in general independent of the orientation of the nuclear sites in the sample and therefore can be taken out of the integral of equation (6).

The quantity $P(\nu)$ is called the resonance signal at frequency ν. The integration in the above equation is over those elements of solid angle $d\Omega(\nu)$ such that $\nu<\nu'<\nu+d\nu$ where ν' is given by equation (5). It is important to realize that $d\Omega(\nu')$ is in general a multi-valued function of ν', because there can be several different values of μ and ϕ which yield the same resonance frequency ν'.

2.1 Nuclear Quadrupole Interaction

Nuclei with spin I greater than 1/2 possess an electric quadrupole moment which can interact with the gradient of any electric field existing at the nucleus. The nuclear spin I is taken to be half-integral in this paper. The Hamiltonian of the nuclear quadrupole interaction is [3]

$$\mathcal{H}_Q = \frac{e^2 Qq}{4I(2I-1)}[3I_z^2 - I^2 + \eta(I_x^2 - I_y^2)] \tag{7}$$

where $q=(1/e)V^{zz}$, $\eta=(V^{xx}-V^{yy})/V^{zz}$ $(0\le\eta\le1)$. The quantites V^{xx}, V^{yy} andV^{zz} are the three principal values of the electric field gradient tensor and I_α (α=x,y,z) are spin operators evaluated in the coordinate system in which the field gradient tensor is diagonal. The quantity Q is that component of the nuclear quadrupole moment tensor which, in its principal axis system, is the largest in magnitude. The term $Q_{cc}=e^2Qq$ is referred to as the quadrupole coupling constant, and the asymmetry parameter of the electric field gradient is given by η.

The contribution to the $|m> \leftrightarrow |m-1>$ NMR transition for the $\mathcal{H}_Q$ to be treated as the first-order perturbation of the Zeeman Hamiltonian is [3,4]

$$\nu_{m\leftrightarrow m-1}=\nu_0-\nu_Q[\frac{1}{2}(3\cos^2\theta-1)-\frac{\eta}{2}\sin^2\theta\cos2\phi](m-\frac{1}{2}) \tag{8}$$

where ν_0 is Zeeman transition frequency, $\nu_Q=3e^2qQ/[2I(2I-1)h]=3Q_{cc}/[2I(2I-1)h]$.

When I is half-integral, the central transition ($m=1/2\leftrightarrow m=-1/2$) shows an unshifted resonance location, which is independent of the direction of the field gradient tensor principle axis with respect to the magnetic field. The satellite lines are flanked at equal distances. The amount of shift of the satellite lines for the first-order perturbation is proportional to ν_Q and relevant to the direction of the principal axis of the crystal electric field gradient tensor with respect to the applied magnetic field. The magnitude of the scanning range is the same order of magnitude of ν_Q. The example of nucleus with I=3/2 and η=0 is shown in figure 1.

The dashed line expresses the powder pattern obtained by introducing the resonance condition, equation (8), into the space-averaging integration equation (6). The solid line is the experimental spectrum of ^{23}Na NMR for the $NaNO_3$ powdered sample. As shown in figure 1, the total area under the satellite line shape to that under the central line shape should be 3:2. The width of the central line shape (narrow line shape) is of the order of several 10 kHz's, but the width of the satellite line shape is of the order of magnitude of 1 MHz. So, within the scanning region of the central transition line shape, the absorption intensity contributed by the satellite transition is negligible. This study only considers the central transition and neglects the contribution of satellite transitions.

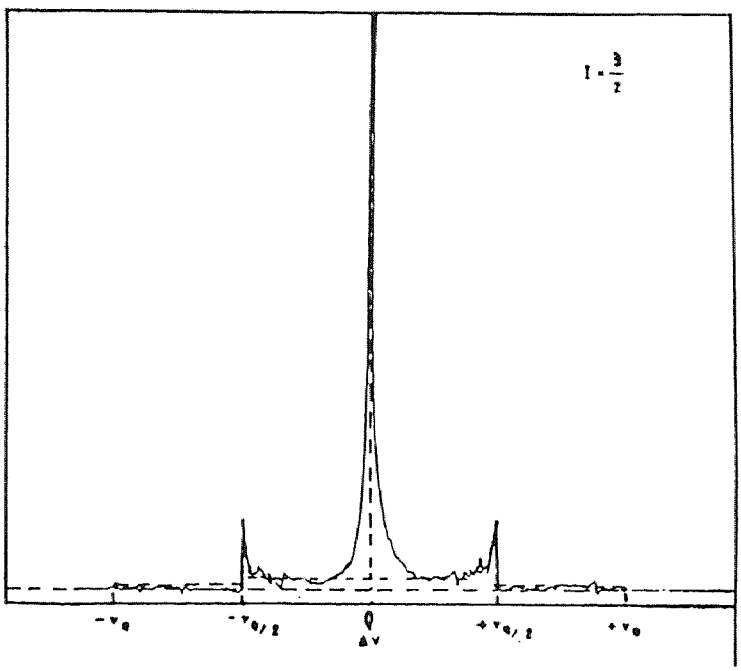

Figure 1 The powder pattern for the case of I=3/2, η=0. The solid line indicates the experimental spectrum of $^{23}NaNO_3$, and the dashed line indicates the theoretical spectrum with a first-order quadrupolar effect. The experimental spectrum of $^{23}NaNO_3$ was obtained from an MSL-300 spectrometer in the East China Normal University.

Treating the nuclear quadrupole interaction as a perturbation for the nuclear Zeeman energy of second order, the central transition line is shifted [3,4]

$$\nu_{1/2\leftrightarrow -1/2}=\nu_0-\frac{R}{6\nu_0}[A(\phi)\cos^4\theta+B(\phi)\cos^2\theta+C(\phi)] \tag{9}$$

where

$$R=\nu_Q^2[I(I+1)-3/4]$$

$$A(\phi)=-\frac{27}{8}-\frac{9}{4}\eta\cos 2\phi-\frac{3}{8}\eta^2\cos^2 2\phi$$

$$B(\phi)=\frac{30}{8}-\frac{1}{2}\eta^2+2\eta\cos 2\phi+\frac{3}{4}\eta^2\cos^2 2\phi$$

$$C(\phi)=-\frac{3}{8}+\frac{1}{3}\eta^2+\frac{1}{4}\eta\cos 2\phi-\frac{3}{8}\eta^2\cos^2 2\phi \tag{10}$$

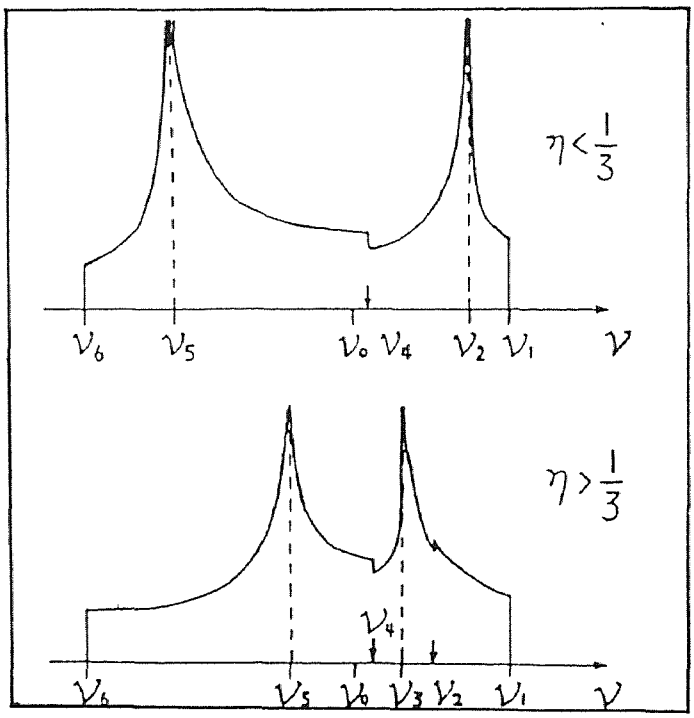

Figure 2 Powder pattern due to the nuclear quadrupole interaction for the central transition (m=1/2↔−1/2) of the NMR of a half-integral nuclear spin. The location of the shoulders and singularities are specified. There are two cases, depending on whether the asymmetry parameter is greater than or less than 1/3.

Using equation (6) and equation (9), a powder pattern due to the effect of the nuclear quadrupole interaction is obtained. Figure 2 shows the powder pattern along with the locations of the shoulders and singularities. There are two different cases, depending on wether η is greater than or less than 1/3.

The locations of the shoulders and singularities of the powder patterns can be obtained by examining the resonance condition equation (9). This equation defines a surface in (μ,ϕ) space, and shoulders and singularities will occur at frequencies that correspond to critical points on the $\nu(\mu,\phi)$ surface. These critical points are found using the conditions [4]

$$(\partial\nu/\partial\mu)_{\mu=a,\,\phi=b} = (\partial\nu/\partial\phi)_{\mu=a,\,\phi=b} = 0 \qquad (11)$$

where (a, b) are the coordinates of a critical point. The nature of the critical point (a,b) is determined by the sign of D [4], where

$$D=[(\partial^2\nu/\partial\mu\partial\phi)^2-(\partial^2\nu/\partial\mu^2)(\partial^2\nu/\partial\phi^2) \qquad (12)$$

If D>0, then (a,b) is the location of a saddle point on the surface, while if D<0, (a,b) corresponds to a local maximum (or minimum). The results for the pure quadrupole interaction are listed in Table 1.

Table 1 Locations of Shoulders and Singularities in a Powder Pattern for the m=1/2↔m= −1/2 Transition Due to Pure Nuclear Quadrupole Interaction

Critical Points of Freq.	$\eta<1/3$	$\eta>1/3$
$\nu_1=\nu_0+R(3+\eta)^2/144\nu_0$	shoulder	shoulder
$\nu_2=\nu_0+R(3-\eta)^2/144\nu_0$	singularity	shoulder
$\nu_3=\nu_0+R(1-\eta^2)/18\nu_0$	none	singularity
$\nu_4=\nu_0+R\eta^2/36\nu_0$	shoulder	shoulder
$\nu_5=\nu_0-R(1-\eta)/9\nu_0$	singularity	singularity
$\nu_6=\nu_0-R(1+\eta)/9\nu_0$	shoulder	shoulder

2.2 Anisotropic Chemical Shift

It is known that the external magnetic field induces a current in the electronic orbitals of a solid. The induced current in turn produces an additional small magnetic field at the nucleus which causes a shift in the resonance condition called the chemical shift. The chemical shift Hamiltonian is [3,7]

$$\mathcal{H}cs=\gamma\hbar\bar{I}\cdot\bar{\bar{\sigma}}\cdot\bar{H}_0 \tag{13}$$

where H_0 is the applied magnetic field, and σ is the chemical shift tensor.

In general, it is sufficient to express $\mathcal{H}_{cs}$ as a first-order perturbation of the Zeeman Hamiltonian. The contribution of $\mathcal{H}_{cs}$ to the shift of the transition $|m> \leftrightarrow |m-1>$ (resonance) is proportional to $<m|\mathcal{H}cs|m> - <m-1|\mathcal{H}cs|m-1>$. The resulting resonance condition is [3,6]

$$\nu=\nu_0[(1-\sigma_1)\sin^2\theta\sin^2\phi+(1-\sigma_2)\sin^2\theta\cos^2\phi+(1-\sigma_3)\cos^2\theta] \tag{14}$$

where $\sigma_1,\sigma_2,\sigma_3$ are the three principal values of the chemical shift tensor.

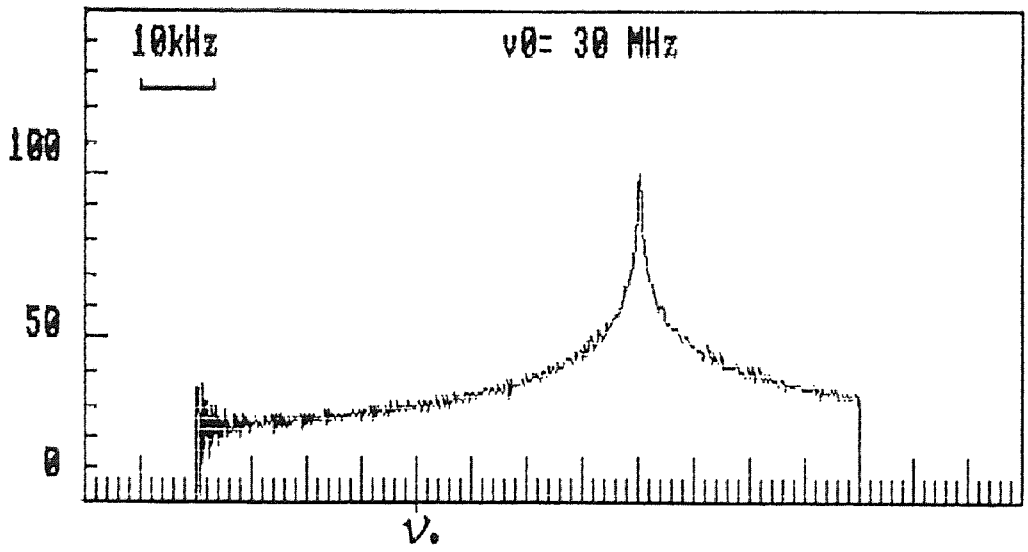

Figure 3 Powder pattern due to the anaxially symmetric chemical shift effect. The locations of the shoulders and singularities are specified. $\nu_1=\nu_0(1-\sigma_1)$, $\nu_2=\nu_0(1-\sigma_2)$, $\nu_3=\nu_0(1-\sigma_3)$.

By substituting the resonance condition of equation (14) into the space-averaging integration equation (6), a corresponding powder pattern is obtained for the contribution of only the chemical shift effect. Figure 3 shows the powder pattern along with the locations of the shoulders and singularities.

2.3 Combined Nuclear Quadrupole and Anisotropic Chemical Shift Effects

If the total interactions include both the nuclear quadrupole interactions and the chemical shift effects, the total Hamiltonian is

$$\mathcal{H}=\mathcal{H}_Z+\mathcal{H}_{CS}+\mathcal{H}_Q$$

The resonance condition is obtained by adding together the first-order resonance condition for the chemical shift and both the first-order and second-order resonance condition for the nuclear quadrupole interaction. The shift of the resonance location is then proportional to

$$\langle m|\mathcal{H}_{CS}+\mathcal{H}_Q|m\rangle-\langle m-1|\mathcal{H}_{CS}+\mathcal{H}_Q|m-1\rangle$$

$$+\sum_{m'}\ [\langle m|\mathcal{H}_Q|m'\rangle\langle m'|\mathcal{H}_Q|m\rangle]/(E_m-E_{m'})$$

$$-\sum_{m''}\ [\langle m-1|\mathcal{H}_Q|m''\rangle\langle m''|\mathcal{H}_Q|m-1\rangle]/(E_{m-1}-E_{m''})$$

Therefore, the resonance condition of the central transition ($\frac{1}{2}\leftrightarrow-\frac{1}{2}$) can be obtained for spin I with half-integral [3]

$$\nu_{1/2\leftrightarrow -1/2}=\nu_0[(1-\sigma_1)\sin^2\theta\sin^2\phi+(1-\sigma_2)\sin^2\theta\cos^2\phi+(1-\sigma_3)\cos^2\theta]$$

$$-\frac{R}{6\nu_0}[A(\phi)\cos^4\theta+B(\phi)\cos^2\theta+C(\phi)] \qquad (15)$$

The resonance condition of equation (15) is substituted into the space-averaging integration equation (6) to get the powder pattern of the central transition due to the combined second order nuclear quadrupole interactions and

first order chemical shift effects. Figure 4 shows the powder patterns. The critical point ν_3 does not appear in the figure because of $\eta<\frac{1}{3}$

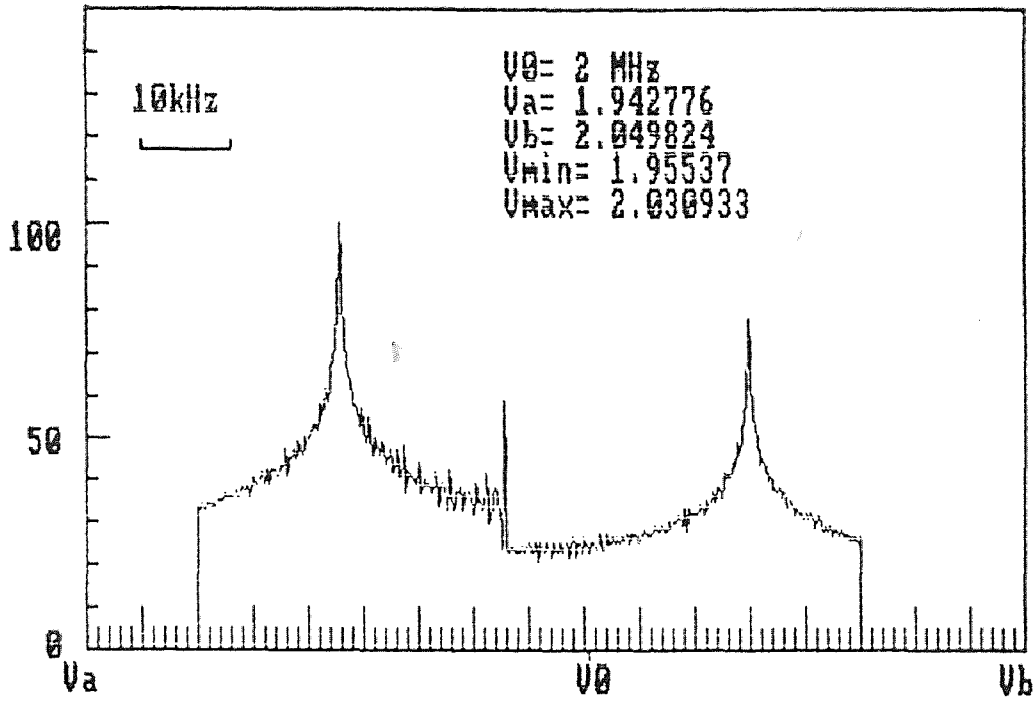

Figure 4 Powder pattern for the central transition in the presence of quadrupole interactions and chemical shift effects at the applied resonance frequency ν_0=2.0 MHz. Parameters are Q_{cc}=2.8 MHz, η=0.2, σ_1=-4.8×10^{-3},σ_2=-0.8×10^{-3}, σ_3=4.8×10^{-3}. The locations of shoulders and singularities are indicated. ν_3 does not appear because of $\eta<\frac{1}{3}$

Using equations (11), (12) and (15), the locations of the critical points of the corresponding powder pattern can be calculated and the nature of the critical points can be determined as shown in Table 2

Table 2 Locations of Shoulders and Singularities in Powder Pattern for $m=1/2 \leftrightarrow -1/2$ Transition

Crytical Points of Frequency	Critical Points of μ and ϕ
$\nu_1=\nu_0+R(3+\eta)^2/144\nu_0-\sigma_1\nu_0$	$\cos\theta=0$; $\cos2\phi=-1$
$\nu_2=\nu_0+R(3-\eta)^2/144\nu_0-\sigma_2\nu_0$	$\cos\theta=0$; $\cos2\phi=+1$
$\nu_3=\nu_0+R(1-\eta^2)/18\nu_0-\frac{1}{2}[1+(3\eta)^{-1}]\sigma_2\nu_0$ $-\frac{1}{2}[1-(3\eta)^{-1}]\sigma_1\nu_0-(\sigma_2-\sigma_1)^2\nu_0^3/\eta^2R$	$\cos\theta=0$; $\cos2\phi=(3\eta)^{-1}+4(\sigma_2-\sigma_1)\nu_0^2/\eta^2R$
$\nu_4=\nu_0+R\eta^2/36\nu_0-\sigma_3\nu_0$	$\cos2\phi=[(2\sigma_3-\sigma_1-\sigma_2)\nu_0-(6+\eta^2)R/6\nu_0]$ $\div[5\eta R/6\nu_0+(\sigma_2-\sigma_1)\nu_0]$; $\cos\theta=\pm1$
$\nu_5=\nu_0-[(5-\eta)\sigma_3+2(2-\eta)\sigma_1]\nu_0/3(3-\eta)$ $-R(1-\eta)/9\nu_0-4(\sigma_3-\sigma_1)^2\nu_0^3/(3-\eta)^2R$	$\cos2\phi=-1$; $\cos^2\theta=(5-\eta)/3(3-\eta)$ $+8(\sigma_3-\sigma_1)\nu_0^2/(3-\eta)^2R$
$\nu_6=\nu_0-[(5+\eta)\sigma_3+2(2+\eta)\sigma_2]\nu_0/3(3+\eta)$ $-R(1+\eta)/9\nu_0-4(\sigma_3-\sigma_2)^2\nu_0^3/(3+\eta)^2R$	$\cos2\phi=+1$; $\cos2\theta=(5+\eta)/3(3+\eta)$ $+8(\sigma_3-\sigma_2)\nu_0^2/(3+\eta)^2R$

2.4 Dipole-Dipole Interaction

The powder pattern already discussed has been obtained without the effects of the dipole-dipole interactions. This interaction will broaden and smooth out the theoretical powder pattern. The actual absorption line shape functions will be given by convoluting these powder patterns with isotropic broadening functions of the appropriate linewidth due to the dipole-dipole interactions [3,5].

$$S(\nu)=\int_{-\infty}^{+\infty}P(\nu')F(\nu-\nu')d\nu' \tag{16}$$

Generally, the normalized Gaussian function, $F(\nu-\nu')$, is used to account for the dipolar broadening mechanism,

$$F(\nu-\nu')=\frac{1}{2\sigma^2\pi^{1/2}}\exp[-\frac{(\nu-\nu')^2}{2\sigma^2}] \tag{17}$$

where 2σ is refered to as the "dipolar width" and is equal to the peak-to-peak width of the derivative of the $F(\nu-\nu')$ broadening function.

An example of convoluting the powder pattern with the dipolar broadening effect is shown in figure 5.

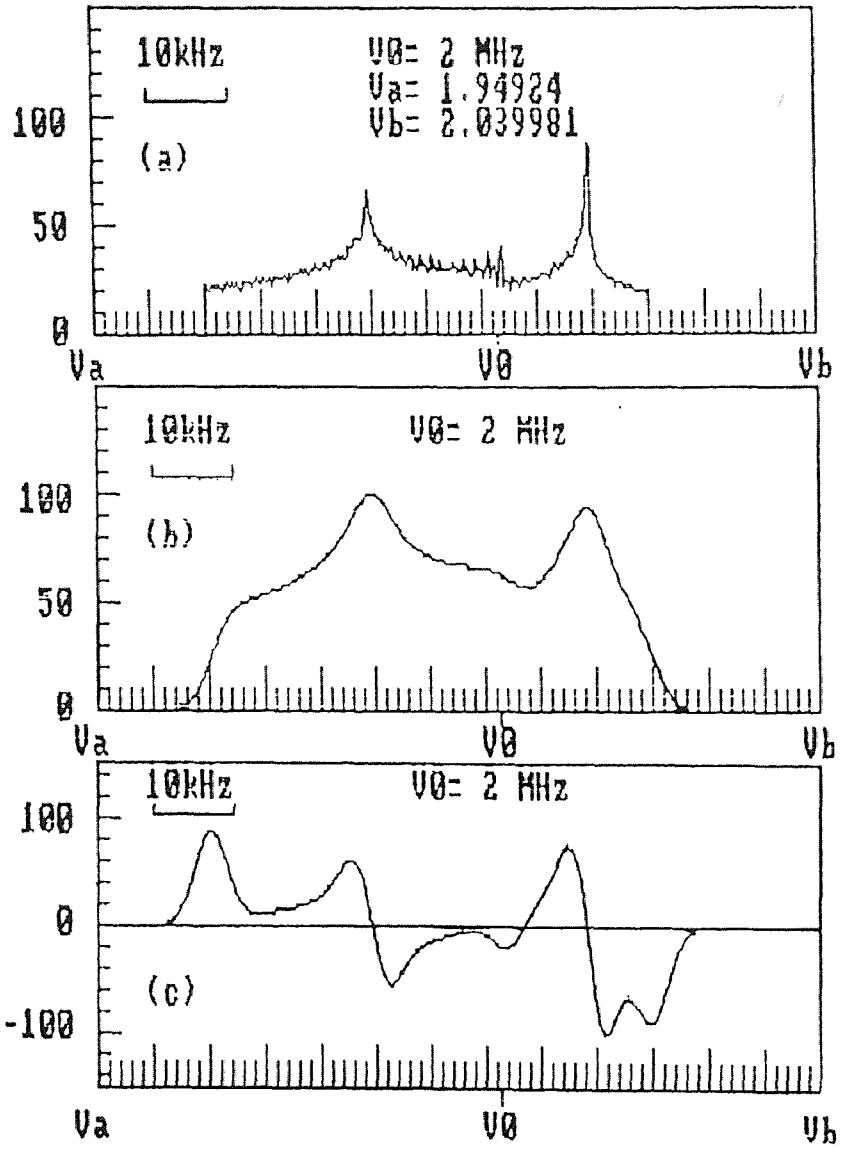

Figure 5 (a) Powder pattern with η=0.5.
(b) Convoluted absorption spectrum.
(c) Derivative of the absorption spectrum of (b).

Figure 5(a) is the ^{51}V NMR powder pattern with parameters Q_{cc}=0.8 MHZ,η=0.38. Figure 5(b) expresses the convolution result of Figure 5(a) due to the effects of dipolar broadening upon the powder pattern. The S(ν) shape function expresses the actual experimental NMR absorption spectrum. Figure 5(c) shows the derivative spectrum of the absorption spectrum.

Experimentally, the derivative-like spectra are obtained by modulation techniques commonly used in NMR. The derivative with respect to frequency ν of the theoretical absorption line shape is used to simulate the actual experimental NMR derivative spectrum. Agreement between the computed and experimental NMR spectra can be obtained by adjusting the parameters ν_Q, η (for nuclear quadrupole interactions); σ_1, σ_2, σ_3 (for chemical effects); and 2σ (for dipole-dipole interactions).

CHAPTER 3

COMPUTER SIMULATION TECHNIQUE

In general, when a certain type of nuclear spin is considered for several different environments, each corresponds to a set of Hamiltonian parameters (ν_Q, η, σ_1, σ_2, σ_3, 2σ). For example, the BO_4 tetrahedral unit and BO_3 triangle unit are two kinds of network units [7] where ^{11}B experiences different environments for each of the two network units, and each one corresponds to a powder pattern. In order to obtain a simulation spectrum, the procedure is as follows:

The first step in simulating an experimental spectrum is to compute the powder patterns for all the components of the appropriate resonance spectrum.

The second step is to convolute these powder patterns with isotropic broadening functions of the appropriate linewidths.

The third step is to add together these convoluted spectrum components with appropriate weighting factor for each and get the total absorption spectrum which simulates the experimental absorption spectrum of the sample.

The final step requires that the derivative of the convoluted spectrum be taken and the resulting trace displayed graphically.

The resonance conditions and transition probabilities discussed in above section are used to evaluate the powder pattern for each allowed transition and can be written in the following generalized form

$$\nu=F(\mu, \phi, \nu_0, \nu_Q, \eta, \sigma_1, \sigma_2, \sigma_3)$$

The NMR absorption powder pattern of the powdered sample is obtained by averaging equation (6) over all elements of solid angle. This averaging is done numerically. The numerical summation is used instead of integration equation (6) by using a finite small solid angle element $\Delta\Omega(\nu)$, $\Delta\Omega=\Delta\mu\cdot\Delta\nu$, instead of the

differential solid angle element $d\Omega(\nu)$, and a finite small frequency step $\Delta\nu$ instead of the differential frequency step $d\nu$. So, instead of using integral equation (6), the numerical summation is as shown in equation (18) and Figure 6, where $\Delta\Omega_k = 4\pi/N$.

$$P(\nu i) = \frac{1}{4\pi \cdot \Delta\nu} \sum_{k=1}^{N} \Delta\Omega_k(\nu) \tag{18}$$

$$\nu_i - \Delta\nu/2 \le \nu \le \nu_i + \Delta\nu/2 \tag{19}$$

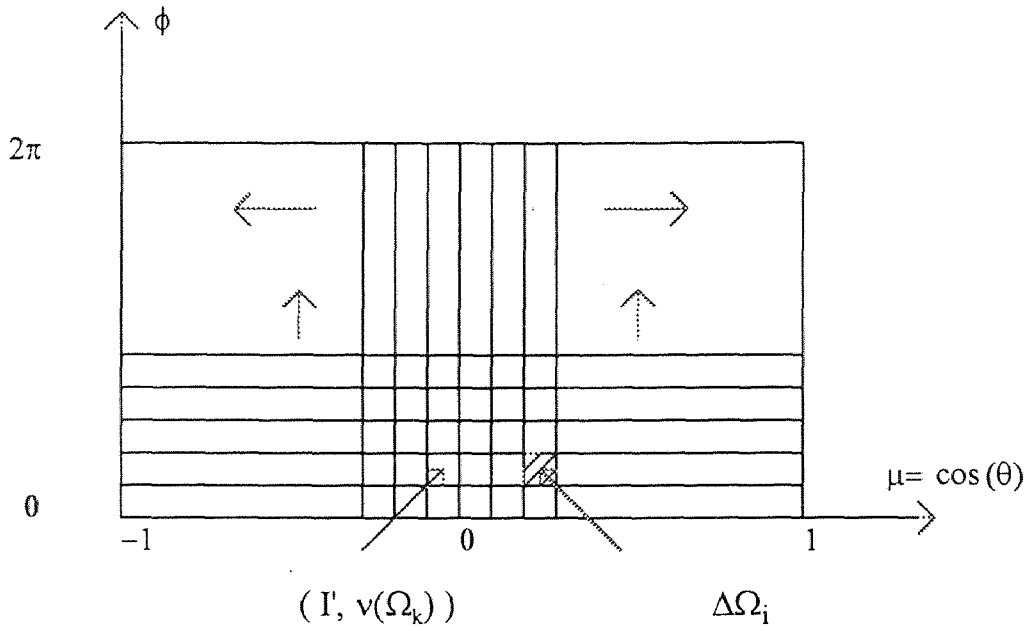

Figure 6a. The grids of $\mu-\phi$ space are uniformly divided into N' solid angle elements where μ $(-1\leftrightarrow+1)$ space is equally separated into N_2' units, and ϕ $(0\leftrightarrow 2\pi)$ N_3' units. Thus $N'=N_2'\times N_3'$. It is assumed that the resonance frequency and transition probability for the elements of solid angle $\Delta\Omega_k$ are evaluated at the center of that element. Because ν is an even function of μ, the μ-value is confined in the region $(0\leftrightarrow 1)$. Similarly, the ϕ-value is confined in the region $(0\leftrightarrow\pi/2)$. The number of uniformly divided grids was N $(=N_2\times N_3)$.

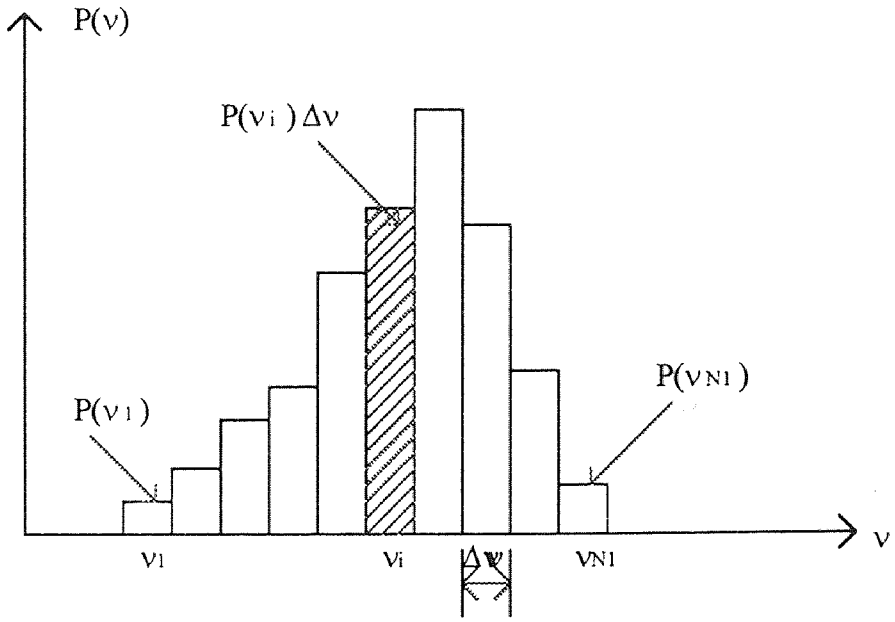

Figure 6b. The rectangle spectrum was obtained using equation (18). The absorption intensity at the frequency position ν_i was $P(\nu_i)$. The area of a rectangle $P(\nu_i)\cdot\Delta\nu$ indicates the absorption intensity between $\Delta\nu$ at the frequency position ν_i. The frequency region of the spectrum ($\nu_{min}\leftrightarrow\nu_{max}$) was divided into N_1 units. Total area surrounded by the curve was $\{P(\nu_1)+P(\nu_2)+\ldots+P(\nu_{N1})\}\cdot\Delta\nu$

The resonance frequency and transition probability for the elements of solid angle $\Delta\Omega_k$ are evaluated at the center of that element. $P(\nu_i)$ is the intensity value of the powder pattern at position of frequency ν_i . The constant factor outside of the summation note in equation (18) can be disregarded because the resulting powder pattern should be normalized.

Also, the numerical summation is used instead of the integral equation (16) for convolution

$$S(\nu_l)=\sum_{i=1}^{N} P(\nu_i)\cdot F(\nu_l-\nu_i)\cdot\Delta\nu \qquad (20)$$

The starting point and end point are respectively l=1-k and l=1+k where the value k is adjustable and is adjusted according to the convolution width 2σ. In general, the value is chosen to just let the intensity of powder pattern outside the frequency region (l=1−k, l=1+k) be small enough to be omited.

This computer simulation program is developed for an IBM PC 486 computer by using Fortran 77. The powder pattern, the convoluted absorption spectrum and the derivative spectrum are calculated and obtained by this computer program.

The computer program is verified for its correctness by the following fact. When only the chemical shift effects are considered, the exact analytical expression of the powder pattern can be obtained. In the case of an axially symmetric chemical shift ($\nu_{11}=\nu_{22}=\nu_{\perp}$, $\nu_{33}=\nu_{//}$; $\nu_{11}=\sigma_1\cdot\nu_0$, $\nu_{22}=\sigma_2\cdot\nu_0$, $\nu_{33}=\sigma_3\cdot\nu_0$), the corresponding powder pattern is expressed as [6]

$$P(\nu)=\frac{1}{2}[(\nu_{//}-\nu_{\perp})(\nu-\nu_{\perp})]^{-1/2} \tag{21}$$

In the case of the anaxially symmetric chemical shift (supposing that $\nu_{33}>\nu_{22}>\nu_{11}$), the corresponding powder pattern is expressed as [6]

$$P(\nu)=\pi^{-1}(\nu-\nu_{11})^{-1/2}(\nu_{33}-\nu_{22})^{-1/2}\cdot K(m) \tag{22}$$
$$m=(\nu_{22}-\nu_{11})(\nu_{33}-\nu)/(\nu_{33}-\nu_{22})(\nu-\nu_{11}) \qquad \text{for } \nu_{33}\geq\nu\geq\nu_{22}$$

$$P(\nu)=\pi^{-1}(\nu_{33}-\nu)^{-1/2}(\nu_{22}-\nu_{11})^{-1/2}\cdot K(m) \tag{23}$$
$$m=(\nu-\nu_{11})(\nu_{33}-\nu_{22})/(\nu_{33}-\nu)(\nu_{22}-\nu_{11}) \qquad \text{for } \nu_{22}\geq\nu\geq\nu_{11}$$
$$P(\nu)=0 \qquad \text{for } \nu>\nu_{33} \text{ and } \nu<\nu_{11}$$

$$K(m)=\int_0^{\pi/2} d\phi(1-m^2\sin^2\phi) \tag{24}$$

As shown in figure 7a, the curve of the powder pattern obtained by the exact analytical expression of equation (21) is shown by small circles, and the curve of the same powder pattern drawn by solid smooth line is obtained by the computer

simulation program. The values for the parameters are ν_0=10MHZ,$\sigma_1=\sigma_2=\sigma_\perp$=–0.001 , $\sigma_3=\sigma_{//}$=0.002.

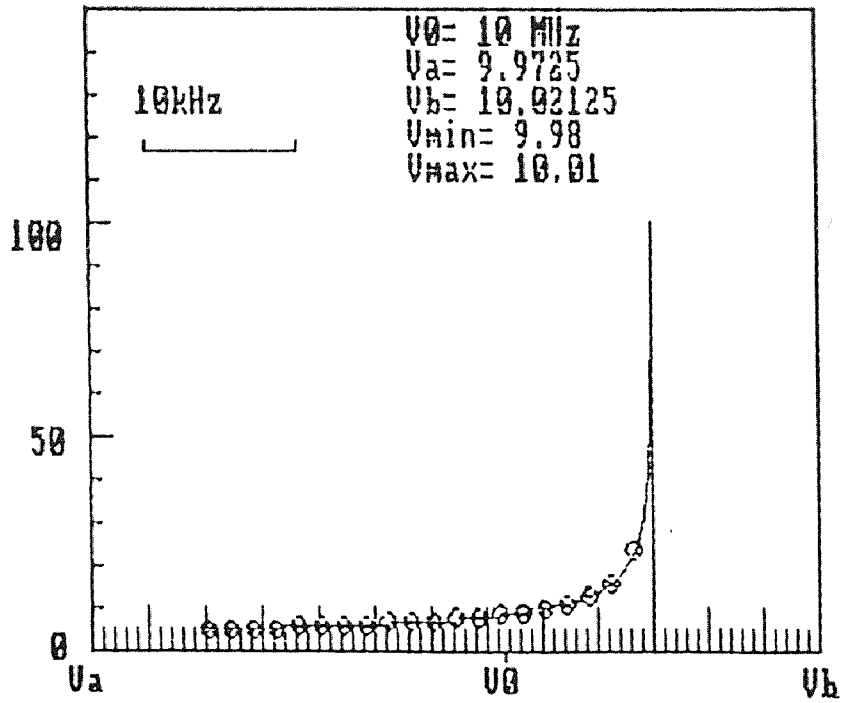

Figure 7a The case of an axially symmetric chemical shift. The small circle curve is obtained through the exact analytical expression, and the solid smooth line is obtained through the computer simulation program.

As shown in figure 7b, the curve of the powder pattern shown by small circles is obtained using the exact analytical expressions of equations (22), (23), and (24). The curve of the same powder pattern drawn by the solid smooth line is obtained by the computer simulation program. The parameters have the following values, ν_0=10 MHZ, σ_1=–0.001, σ_2=0.001, σ_3=0.004.

From figure 7a and figure 7b, it is shown that the powder patterns obtained by the exact analytical expressions are in good agreement with those obtained by the computer simulation program.

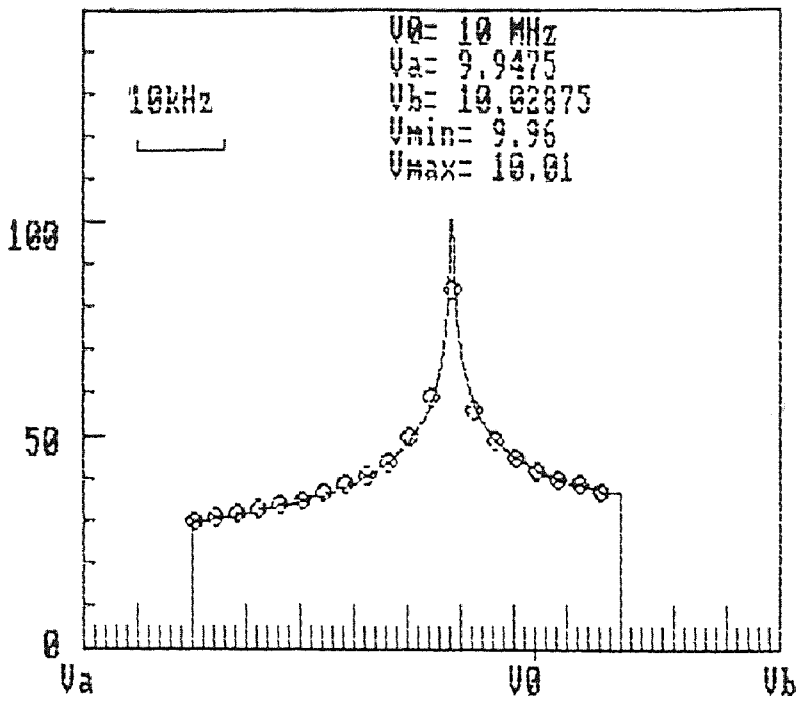

Figure 7b The case of anaxially symmetric chemical shift. Small circle curve is obtained through the exact analytical expression. Solid smooth curve is obtained through computer simulation program.

CHAPTER 4

EXPERIMENTAL

Forty-four glass samples were made throughout the glass-forming region reported by O. B. Маэурнн, et.al.. The compositions were chosen so as to group them into five families of glass samples, each family having the same K value but different R values, as shown in table 5. The values of K and R are indicated by K=mol%V_2O_5/mol%B_2O_3 and R=mol%Na_2O/mol%B_2O_3 for the ternary system glass $xNa_2O{\cdot}yB_2O_3{\cdot}zV_2O_5$. Reagent grade sodium carbonate (Na_2CO_3), orthoborate acid (H_3BO_3) and Vanadium oxide (V_2O_5) were thoroughly mixed in the appropriate proportions, placed in a platinum crucible, and fused at approximately 1100 °C in an electric muffle furnace. After all air bubbles disappeared, the melts were poured onto a metal plate and quickly covered with a brass block. All glass samples were observed to be transparent, were ground into a fine powder, and sealed in polystyrene vials for the NMR study.

A wide-line NMR Spectrometer (HC-4) connected with a Signal Averager was employed to detect the NMR signal of ^{11}B for the glass samples. The NMR spectra were obtained at a fixed frequency of 30 MHz by sweeping the magnetic field through the resonance condition. The scanning range of the field was 0.008 Tesla and the time period for each scan about 3 minutes. The frequency of the modulation field was 32 Hz and the amplitude of the modulation field about 0.0003 Tesla. All measurements were made with the glass samples at room temperature.

The computer simulation of the ^{11}B NMR spectra for the glass samples are discussed in chapter 5.

CHAPTER 5

DISCUSSION OF RESULTS AND EXAMPLES

In this chapter, the noise and accuracy are analyzed, the simulation procedure and examples are discussed, and applications of the NMR computer simulation in the study of glassy and powdered samples are presented.

5.1 Noise in Computer Simulation of Powder pattern

Computer simulation techniques provide expeditious means for comparing experiment with theoretical expectation. But, the computer simulation spectra are not always in accurate agreement with the experimental spectra and if enough of the relevant factors are considered, these differences will be small. In actual powder samples, all "nuclear sites" have orientations which are totally random in angular space. For the computer simulation model, the 4π angular space is divided into a finite number of uniform grids, so, the experimental result will only approximate that of the theoretical model. If more orientations in angular space are taken in the computer simulation, that is, if the $\cos\theta-\phi$ space (4π) is divided into a very large number of uniform grids, the experimental spectra can be accurately simulated by the computer simulation spectra.

Figure 8a shows a ^{11}B NMR computer simulation powder pattern obtained by adding together the resonances due to over 2500 orientations (N_2=100, N_3=25) in $\cos\theta-\phi$ space where $\cos\theta$ ranges from 0 to 1 and ϕ from 0 to π. The pattern contains 100 equal-sized intervals in frequency. Only the nuclear quadrupole interaction is considered for the powder pattern. The resonance frequency condition ν_0 is chosen as 30 MHZ, e^2qQ (Q_{cc}) the nuclear quadrupole coupling

constant as 2.58 MHZ, η the electrical field gradient asymmetry parameter as 0.14 and I the nuclear spin as 3/2.

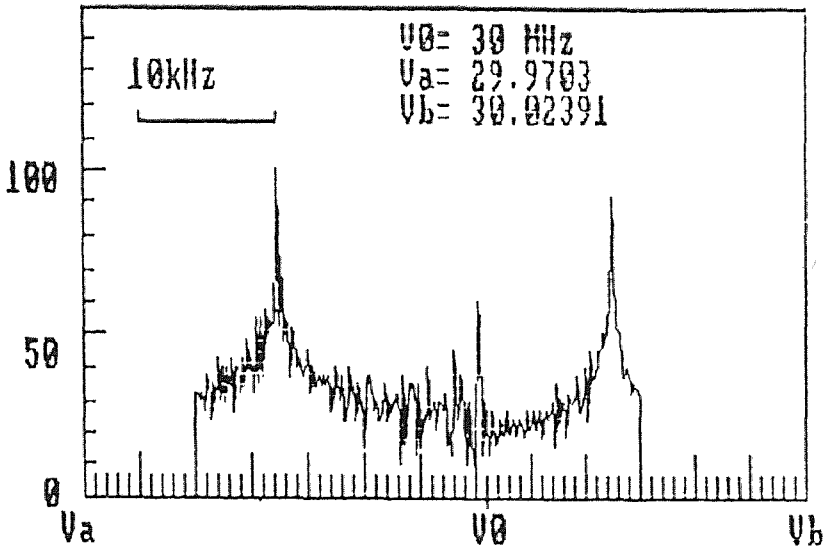

Figure 8a ^{11}B powder pattern with condition, ν_0=30MHz, Q_{cc}=2.58 MHz, η=0.14, I=3/2, N_1=100, N_2=100,N_3=25.

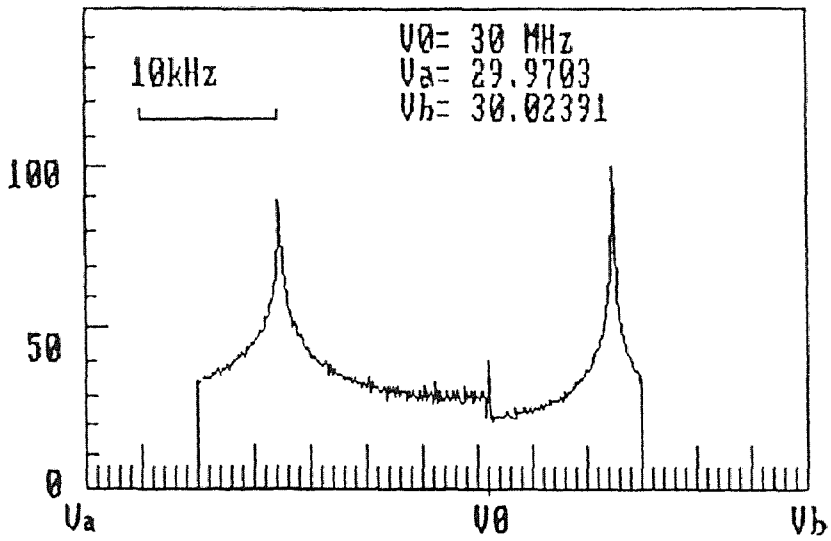

Figure 8b ^{11}B powder pattern with condition, ν_0=30 MHz, Q_{cc}=2.58 MHz, η=0.14, I=3/2, N_1=100, N_2=400, N_3=200.

It is noted that the "noise" of the powder pattern is appreciable in figure 8a. The "noise" appearing in the powder pattern formed from uniform grids tends to be periodic. If the resonance surface is plotted as a function of $\cos\theta$ and ϕ according to resonance conditions of equation (9), or equation (15), then the periodic noise of the powder pattern is observed to come from those regions of the resonance surface which have the strongest dependence on $\cos\theta$ and ϕ. That is, the regions of $\cos\theta-\phi$ space where the slope of the resonance surface is the greatest contibute the most "noise" to the powder pattern. If the "noise" is too large, the signal-to-noise ratio will be severely affected and a weak real signal will be unable to be observed. The resulting resolution of the powder pattern under these conditions is poor.

The "noise" results from the coarseness of the "grid" used in constructing the powder pattern. It can be noted that if the $\cos\theta-\phi$ space is divided into much finer uniform grids, then the noise tends to diminish. Figure 8b shows the powder pattern with the same resonance condition and Hamiltonian parameters as that in figure 8a, but, the $\cos\theta-\phi$ space is divided into 80000 uniform grids (or orientations), that is, $N_2=400, N_3=200$. Obviously, the "noise" of the powder pattern in figure 8b is much weaker than that in figure 8a.

In practice, the noise level can not diminish completely, because the number of grids for $\cos\theta-\phi$ space being divided only can be finite. Fortunately, the effect of dipolar broadening will "smooth out" the "noise" of the powder pattern, which depends on the linewidth of the isotropic broadening function used to convolute that powder pattern. In figure 9, the theoretical absorption spectrum $S(\nu)$ is obtained by convoluting the powder pattern in figure 8a by the Gaussian function with the dipolar line width $2\sigma=6$ kHz. This theoretical absorption spectrum is just the parallel to the experimental absorption spectrum.

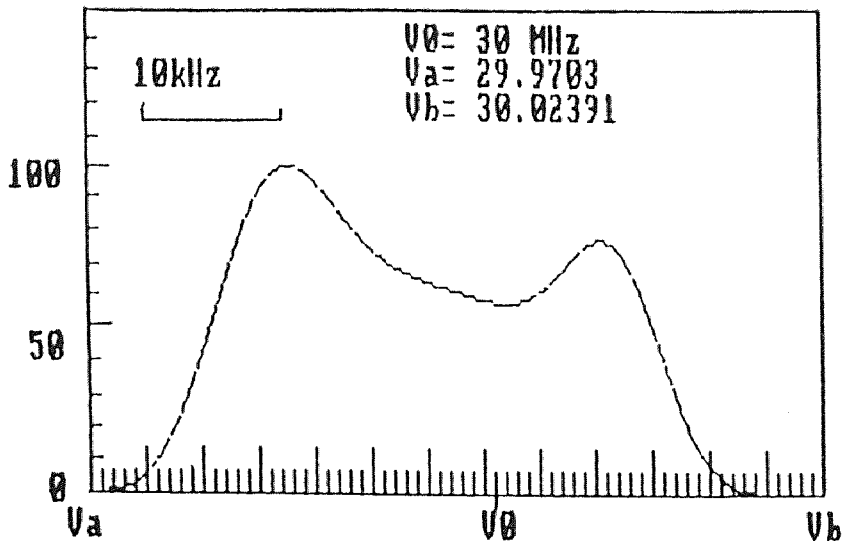

Figure 9 The spectrum S(ν) is obtained by convoluting the powder pattern in figure 8a by a Gaussian function with dipolar line width 2σ=6 kHz.

The relationship between the simulation spectrum "error" brought by spectrum "noise" and the quantity $N=N_2\times N_3$ by which the $\cos\theta-\phi$ space is divided into uniform grids is analyzed. The absorption spectrum is calculated in the situation that only the nuclear quadrupole interaction and dipole-dipole interaction are available in the powder sample. We choose the following parameter values, the nuclear quadrupole coupling constant Q_{cc}=2.58 MHz, the electrical field gradient asymmetry parameter η=0.14, the resonance frequency ν_0=30 MHz, and the Gaussian convolution width 2σ=6 kHz, which are the typical parameter values for the ^{11}B NMR of the boron-oxygen triangle unit BO_{3S}.

We now select the quantity $S_0(\nu)$ to represent the "standard spectrum" which is obtained by dividing frequency spanning range of the pattern into 100 equal-sized intervals (N_1=100), and $\cos\theta-\phi$ space into 80000 uniform grids (N_2=400, N_3=200). Then, different values of N_2 (N_3 value being fixed) or of N_3 (N_2 value being fixed) are taken to obtain the convoluted spectrum S(ν). We can calculate

the relative error between each spectrum $S(\nu)$ and "standard spectrum" $S_0(\nu)$, that is;

$$\Delta E = \frac{\sum_i \left| S(\nu_i) - S_0(\nu_i) \right|}{\sum_i S_0(\nu_i)}$$

$\Delta E \sim N_2$ (N_3 fixed) and $\Delta E \sim N_3$ (N_2 fixed) curves are plotted in figure 10.

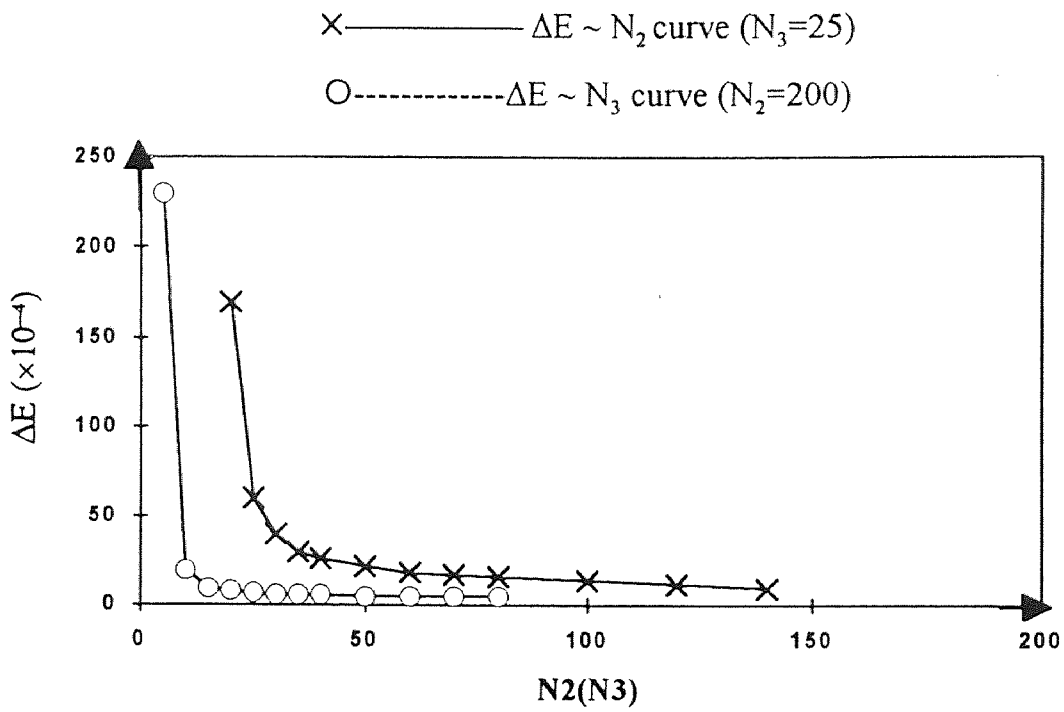

Figure 10 $\Delta E \sim N_2(N_3)$ curves, $\Delta E = \frac{\sum_i \left| S(\nu_i) - S_0(\nu_i) \right|}{\sum_i S_0(\nu_i)}$

N_2 — ($\cos\theta$: $0 \leftrightarrow +1$) number of uniformly divided intervals.
N_3 — (ϕ: $0 \leftrightarrow \pi/2$) number of uniformly divided intervals.

Figure 10 shows that to satisfy the requirements of computer simulation accuracy and reasonable calculation times, values of N_2 of 100 and N_3 of about 25

can be used with confidence to calculate the simulation spectrum of the Hamiltonian parameters (Q_{cc}, η, 2σ, ν_0) which are as approximate as that in the figure 10. These approximations will introduce no apparent additional error into the calculated spectrum.

5.2 Simulation Procedure

In computer program simulation, it is not easy to simultaneously adjust all the Hamiltonian parameters so that the calculated spectra is in good agreement with the experimental spectra; especially when both nuclear quadrupole interactions and chemical shift effects are considered in the powdered samples.

From the resonance condition equations, it is known that the spectrum spanning range width caused only by chemical shift effects is proportional to the applied resonance frequency, that is, $\Delta\nu_{cs} \propto \nu_0$ and the spectrum spanning range width caused only by nuclear quadrupole interactions is proportional to the inversion of ν_0, that is, $\Delta\nu_Q \propto 1/\nu_0$. So, at the applied low resonance frequency, the nuclear quadrupole interactions predominate the anisotropic broadening effects. When the applied resonance frequency is increased, the broadening effects due to the nuclear quadrupole interaction are decreased and the broadening effects due to the chemical shift effects are increased gradually. At the applied high resonance frequency, the chemical shift broadening effects become the main role.

Figure 11 shows five powder patterns in the presence of both nuclear quadrupole interactions and chemical shift effects for the powder sample. The following Hamiltonian parameters of ^{51}V of the $NaVO_3$ sample are chosen: Q_{cc}=3.65 MHz, η=0.6, σ_1=-1.5×10^{-4}, σ_2=0.8×10^{-4}, σ_3=3.4×10^{-4}, and I=7/2. The powder patterns have been calculated for the applied frequencies ν_0=1, 4, 30, 90, and 160 MHz using the computer. These parameters and frequencies are chosen to span the range from nearly pure nuclear quadrupole interaction to nearly pure

chemical shift. Figure 12a shows three powder patterns in the presence of only nuclear quadrupole interactions for the powdered sample with parameters as, Q_{cc}=3.65MHz, η=0.6, and I=7/2, for the applied frequencies ν_0=1, 4 and 30 MHz. Figure 12b shows three powder patterns in the presence of only chemical shift effects for the powdered sample with parameters as, σ_1=-1.5×10^{-4}, σ_2=0.8×10^{-4}, σ_3=3.4×10^{-4} and I=7/2, for the applied frequencies ν_0=30, 90 and 160 MHz.

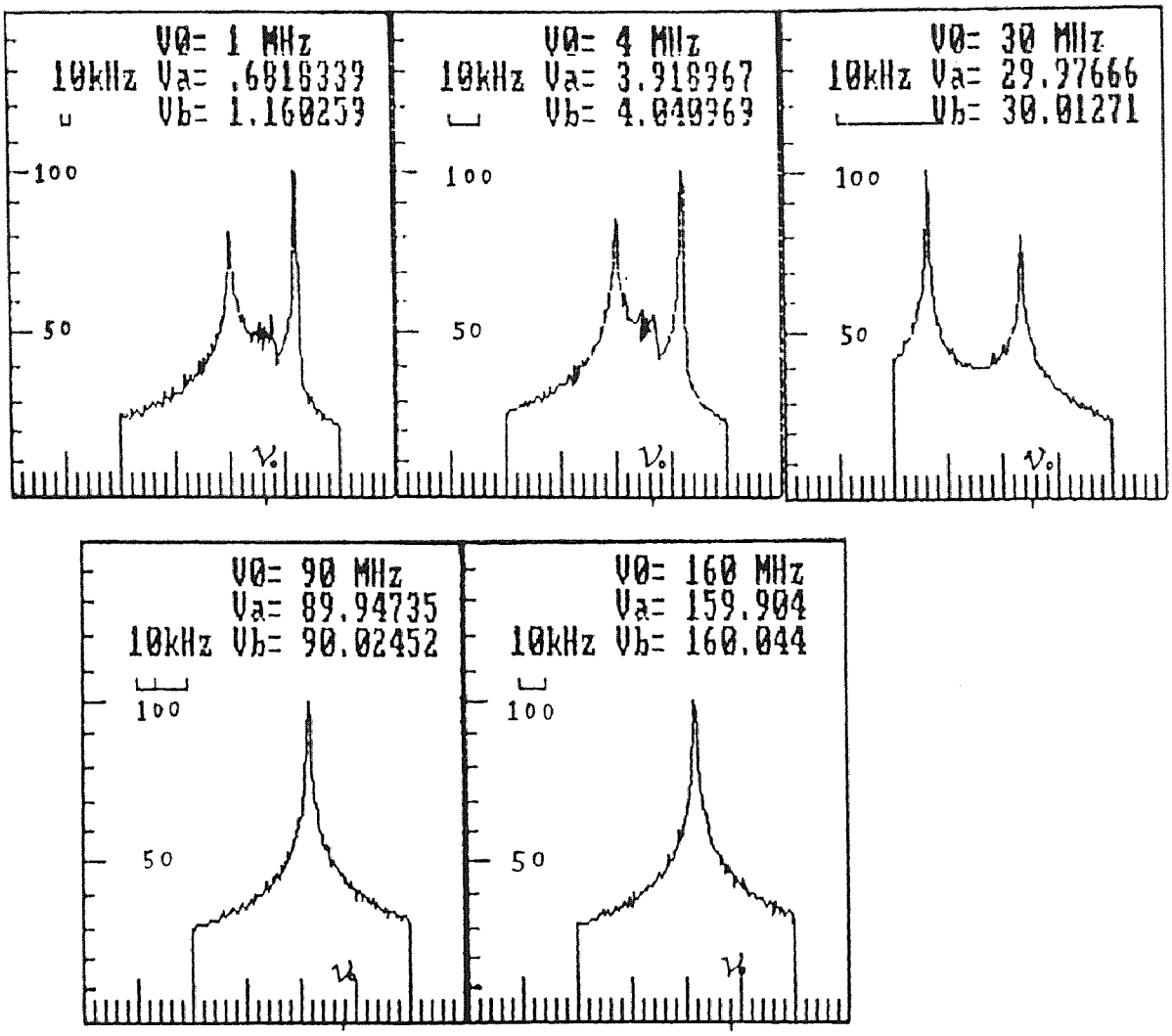

Figure 11 Powder patterns in the coexistence of nuclear quadrupolar interactions and chemical shift effects with parameters as,Q_{cc}=3.65 MHz, η=0.6, σ_1=-1.5×10^{-4}, σ_2=0.8×10^{-4}, σ_3=3.4×10^{-4},and ν_0=1,4,30,90,160 MHz

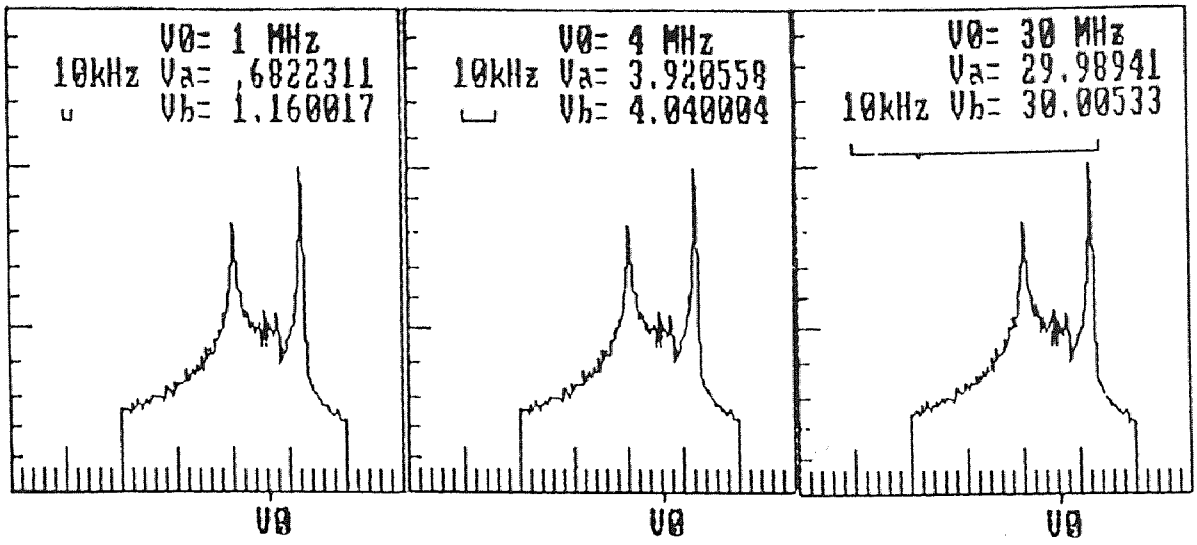

Figure 12a Powder patterns due to only the nuclear quadrupolar interactions with parameters as, Q_{cc}=3.65 MHz, η=0.6, and ν_0=1, 4, 30 MHz.

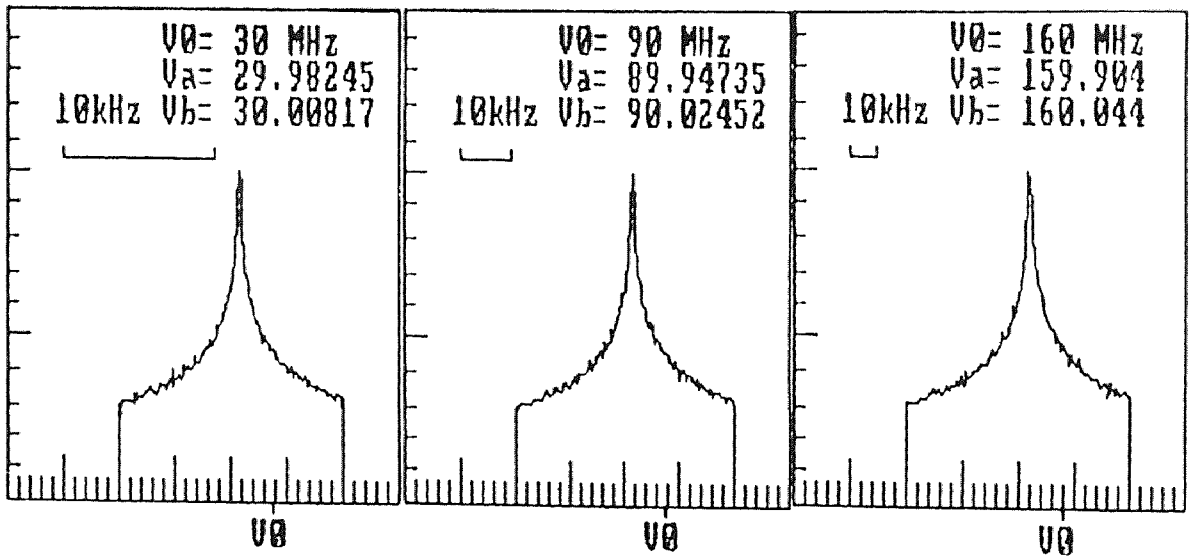

Figure 12b Powder patterns due to only the chemical shift effect with parameters as, σ_1=−1.5×10^{-4}, σ_2=0.8×10^{-4}, σ_3=3.4×10^{-4}, and ν_0=30, 90, 160 MHz.

Comparing figure 11 with figure 12a and figure 12b, it can be concluded that chemical shift effects can be disregarded at the applied low resonance frequencies

, ν_0=1, 4 MHz, and nuclear quadrupole interactions can be disregarded at the applied high resonance frequencies, ν_0=90, 160MHz. But, at the applied medium resonance frequency, ν_0=30 MHz, both nuclear quadrupole interactions and chemical shift effects can not be disregarded.

In the presence of both nuclear quadrupole interactions and chemical shift effects, the procedure used in fitting the experimental spectra can be followed by two steps.

First, by neglecting all chemical shift effects, the values of Q_{cc}, η, and 2σ are estimated from the experimental spectrum taken with lower frequency for which a usable NMR signal can be obtained. In this case, chemical shifts turn out to be really quite small at these low frequencies. This procedure yields a good first estimate of the quadrupole parameters, Q_{cc}, η, and the dipolar width 2σ.

Next, the experimental spectra taken at the higher available frequency are fitted by the adjustment of the three chemical shift parameters (σ_1, σ_2, σ_3) of the calculated spectra. Finally, it is necessary to make small corrections for the low-frequency spectra after chemical shift effects are included. This iterative procedure is continued until the computed spectra agree with the experimental spectra at all frequencies.

Figure 13 shows the example of computer simulation for simulating ^{11}B NMR of $xLi_2O{\cdot}yB_2O_3{\cdot}zV_2O_5$ ternary system glass samples. Superimposed on the experimental derivative spectra are the computed and derivative spectra calculated from the corresponding absorption spectra.

The physical parameters (or, Hamiltonian parameters) obtained by the best fit to the experimental spectra are listed in table 3. The result agree with those obtained by other authors, T. H. Yun, P. J. Bray [7] for the study of $xLi_2O{\cdot}yB_2O_3$ binary system glass samples shown in table 4.

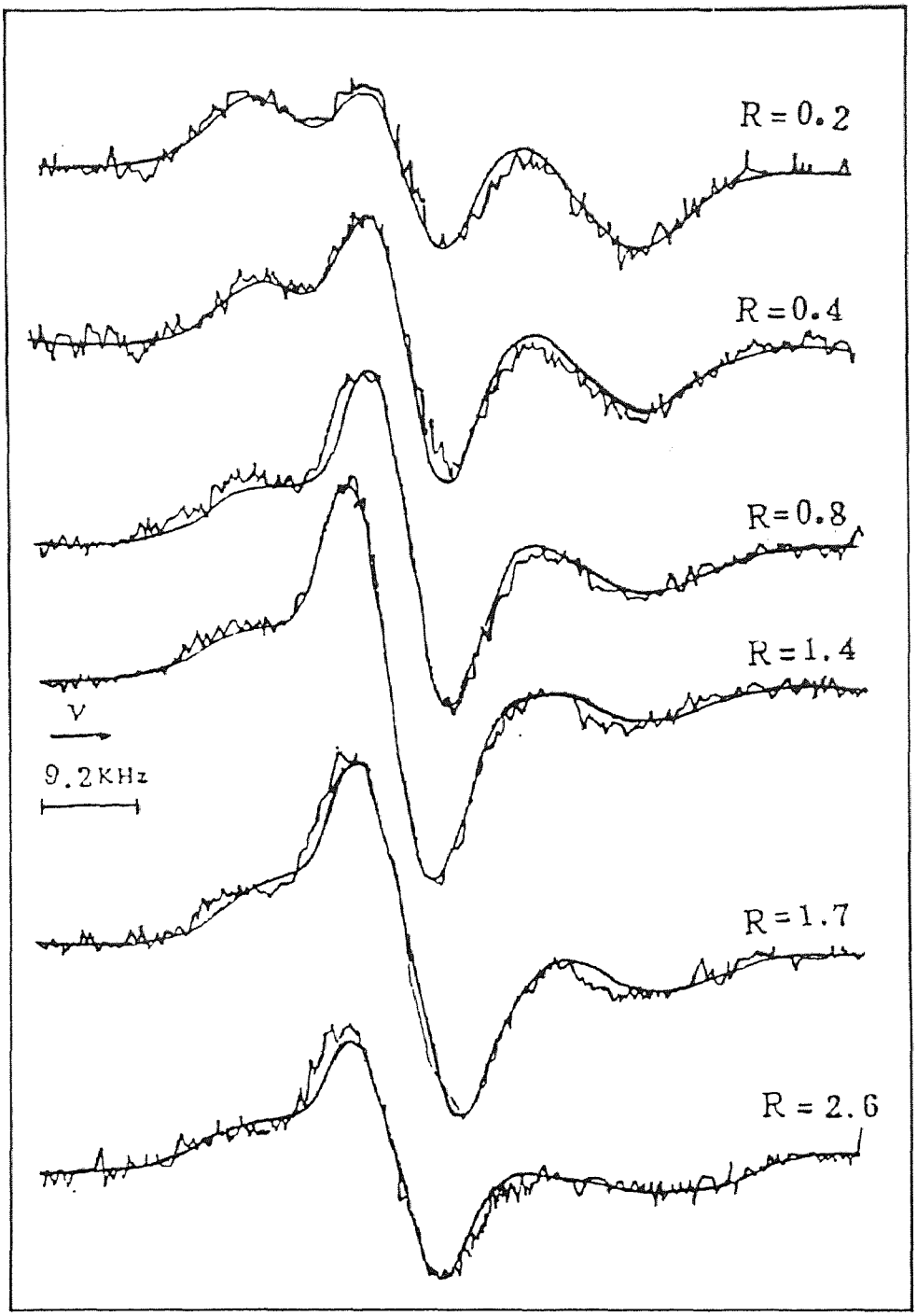

Figure 13 ^{11}B NMR experimental spectra of $xLi_2O{\cdot}yB_2O_3{\cdot}zV_2O_5$ system glass (K=0.4) at a resonance frequency ν_0 of 30 MHz superimposed with the computer simulation spectra (solid smooth curve) R=x/y, K=z/y.

Table 3 The Parameters (Q_{cc}, η, σ) of the Three Distinct Boron Sites in the System of $xLi_2O{\cdot}yB_2O_3{\cdot}zV_2O_5$ Glasses Through Computer Simulation

Samples			Symmetry BO_{3S} unit			Asymmetry·BO_{3A}unit			BO_4 unit		
order	K(z/y)	R(x/y)	Qcc(MHz)	η	σ(kHz)	Qcc(MHz)	η	σ(kHz)	Qcc(MHz)	η	σ(kHz)
1	0.4	0.2	2.61	0.17	4.0	/	/	/	0.5	0	3.5
2	0.4	0.4	2.61	0.17	4.0	/	/	/	0.5	0	3.5
3	0.4	0.8	2.61	0.17	4.0	/	/	/	0.5	0	3.7
4	0.4	1.4	2.64	0.08	4.0	2.61	0.47	4.0	0.5	0	3.7
5	0.4	1.7	2.64	0.08	4.0	2.61	0.47	4.0	0.5	0	3.5
6	0.4	2.6	2.64	0.08	4.0	2.61	0.47	4.0	0.5	0	3.3

Table 4 The Parameters (Q_{cc}, η, σ) of the Two Distinct Boron Sites in the System of $xLi_2O{\cdot}yB_2O_3$ Glasses Through Computer Simulation [7]

Samples		symmetry BO_{3S} unit			Asymmetry BO_{3A} unit		
order	R(x/y)	Q_{cc}(MHz)	η	σ(kHz)	Q_{cc}(MHz)	η	σ(kHz)
1	0.6	2.61	0.14	3.6	2.61	0.45	3.0
2	0.8	2.61	0.13	3.8	2.60	0.49	3.7
3	0.9	2.64	0.08	3.5	2.58	0.47	3.5
4	1.0	2.60	0.08	3.5	2.56	0.50	3.9
5	1.2	2.64	0.10	4.0	2.58	0.47	3.5
6	1.4	2.69	0.08	3.5	2.61	0.47	3.5
7	1.6	2.66	0.08	3.0	2.59	0.50	3.5
8	1.86	2.64	0.08	4.0	2.58	0.47	3.5

The computer simulation is based on the single parameters which are most probable. Actually, the parameter should have some distribution of values around the most probable value for the powdered sample, especially for a vitrious sample. This is another important reason for some disagreement between the calculated and experimental spectrum and this further factor needs to be considered in the computer simulation in order to obtain a better goodness of fit between the calculated and experimental spectra.

5.3 Multiple Sites in the ^{11}B NMR Spectra of Sodium Borovanadate Glasses

In general, separate sites may be characterized by different isotropic broadening function as well as different Hamiltonian parameters. For example, the NMR spectrum of boron in a sodium borovanadate glass consists of three distinct nuclear sites, one corresponding to a boron atom coordinated to four oxygen atoms, and two corresponding to a boron atom coordinated to three oxygen atoms [7]. The single four-coordinated boron site and the two three-coordinated boron sites all have different Hamiltonian parameters and dipolar broadening linewidths which can be uniquely determined by computer simulation techniques. Also, the relative abundances of these three types of boron nuclear sites can be calculated by computer simulation. By determining the relative intensities of the three types of boron nuclear sites, that is, determining the fraction N_4 of BO_4 units with four tetrahedral bridging oxygens, the fraction N_{3S} of BO_{3S} units with three triaganal bridging oxygens and the fraction N_{3A} of BO_{3A} units with one or two non-bridging oxygens (NBO's), the structure of the alkali borate glasses can be studied. In the following two sub-sections, NMR studies are focused on the sodium borovanadate ternary glass by using computer simulation techniques.

5.3.1 Analysis of ^{11}B NMR Spectra of Sodium Borovanadate Glasses by Computer Simulation Techniques

Forty-four glass samples described in chapter 4 are analyzed by ^{11}B NMR and computer simulation. As indicated in chapter 4, ^{11}B spectra of the samples were obtained at a fixed frequency of 30 MHz by sweeping the magnetic field through the resonance by employing wide-line NMR Spectrometer (HC-4).

Figure 14 shows the ^{11}B NMR (derivative) spectrum at a resonance frequency ν_0 of 30 MHz for a sample with K=0.5 and R=0.6. Smooth solid line superimposed on the spectrum in figure 14 is computer-simulated spectrum.

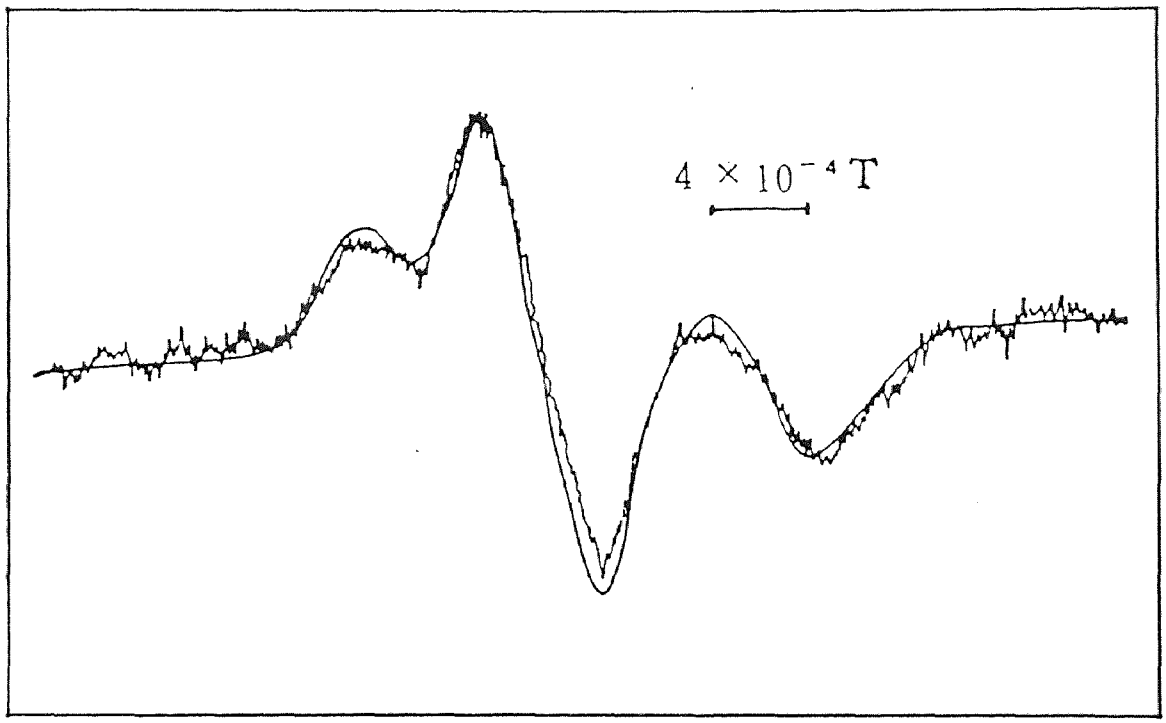

Figure 14 ^{11}B NMR derivative spectrum at a resonance frequency ν_0 of 30 MHz for $xNa_2O{\cdot}yB_2O_3{\cdot}zV_2O_5$ glass with K=0.5 and R=0.6. The smooth solid curve represents a computer-simulated spectrum which are the sums of responses due to three distinct boron sites BO_4, BO_{3S} and BO_{3A}.

The spectrum shows two distinct portions: (1) a narrow line shape due to BO_4 units, and (2) a broad line shape due to BO_3 units. The BO_3 units yield a broad resonance line shape due to a large interaction between the nuclear quadrupole moment and electric field gradient present at the boron site.

By fitting the computer-simulated spectra to experimental spectra, fractions of $N_4(E)$, $N_{3S}(E)$ and $N_{3A}(E)$ can be determined for all the different composition samples (different K and R values). Table 5 shows all the data of fractions of $N_4(E)$, $N_{3S}(E)$ and $N_{3A}(E)$ experimentally determined by computer simulation. In addition, all the data of fractions of $N_4(C)$, $N_{3S}(C)$ and $N_{3A}(C)$ are calculated from the structure model proposed in this paper.

Table 5 Experimental Values of $N_4(E)$, $N_{3S}(E)$ and $N_{3A}(E)$ Determined by Computer Simulation Technique and Theoretical Values of $N_4(C)$, $N_{3S}(C)$ and $N_{3A}(C)$ Calculated from Their Corresponding Compositions According to the Model Proposed in This Paper

Number	K	R	$N_4(E)$	$N_4(C)$	$N_{3S}(E)$	$N_{3S}(C)$	$N_{3A}(E)$	$N_{3A}(C)$
1	0	0.2	0.21	0.20	0.79	0.80	0.00	0.00
2	0	0.3	0.30	0.30	0.70	0.70	0.00	0.00
3	0	0.4	0.37	0.40	0.63	0.60	0.00	0.00
4	0	0.5	0.46	0.50	0.54	0.50	0.00	0.00
5	0	0.6	0.44	0.47	0.38	0.40	0.17	0.13
6	0	0.7	0.43	0.45	0.30	0.30	0.27	0.25
7	0	0.9	0.40	0.40	0.10	0.10	0.50	0.50
8	0	1.5	0.25	0.25	0.11	0.10	0.65	0.65
9	0.5	0.4	0.22	0.22	0.78	0.80	0.00	0.00
10	0.5	0.6	0.31	0.30	0.70	0.70	0.00	0.00
11	0.5	0.9	0.41	0.45	0.60	0.55	0.00	0.00
12	0.5	1.2	0.45	0.46	0.37	0.33	0.18	0.21
13	0.5	1.6	0.37	0.38	0.09	0.00	0.54	0.63
14	0.5	2.0	0.30	0.29	0.09	0.07	0.61	0.64
15	0.5	2.3	0.24	0.23	0.13	0.12	0.63	0.66
16	0.5	2.5	0.21	0.19	0.15	0.15	0.64	0.66
17	0.5	2.7	0.14	0.15	0.20	0.18	0.65	0.67
18	1.0	0.6	0.24	0.12	0.76	0.88	0.00	0.00
19	1.0	0.8	0.29	0.27	0.71	0.73	0.00	0.00
20	1.0	1.0	0.33	0.33	0.67	0.67	0.00	0.00

Table 5 : Continued

Number	K	R	$N_4(E)$	$N_4(C)$	$N_{3S}(E)$	$N_{3S}(C)$	$N_{3A}(E)$	$N_{3A}(C)$
21	1.0	1.4	0.45	0.47	0.55	0.53	0.00	0.00
22	1.0	1.6	0.45	0.48	0.41	0.43	0.15	0.09
23	1.0	1.8	0.43	0.45	0.36	0.29	0.21	0.27
24	1.0	2.0	0.42	0.41	0.26	0.14	0.33	0.45
25	1.0	2.2	0.35	0.37	0.15	0.00	0.50	0.63
26	1.0	2.4	0.34	0.34	0.08	0.03	0.58	0.63
27	1.0	2.6	0.31	0.30	0.08	0.06	0.61	0.64
28	1.0	3.2	0.22	0.20	0.14	0.14	0.63	0.66
29	1.0	3.6	0.15	0.12	0.19	0.20	0.66	0.68
30	1.5	0.8	0.28	0.20	0.73	0.80	0.00	0.00
31	1.5	1.8	0.37	0.45	0.63	0.55	0.00	0.00
32	1.5	2.2	0.48	0.47	0.42	0.38	0.10	0.16
33	1.5	2.6	0.38	0.41	0.23	0.13	0.39	0.47
34	1.5	3.0	0.35	0.35	0.11	0.03	0.55	0.63
35	1.5	3.4	0.31	0.28	0.10	0.08	0.60	0.64
36	1.5	3.8	0.23	0.22	0.12	0.13	0.66	0.66
37	2.0	0.8	0.19	0.16	0.82	0.84	0.00	0.00
38	2.0	1.6	0.34	0.32	0.67	0.68	0.00	0.00
39	2.0	2.0	0.36	0.40	0.65	0.60	0.00	0.00
40	2.0	2.5	0.43	0.50	0.58	0.50	0.00	0.00
41	2.0	3.0	0.45	0.43	0.30	0.22	0.26	0.35
42	2.0	3.5	0.37	0.36	0.09	0.01	0.55	0.63
43	2.0	4.5	0.28	0.22	0.12	0.12	0.60	0.66
44	2.0	5.0	0.18	0.15	0.21	0.18	0.61	0.67

The dependence of the fraction N_4 of BO_4, the fraction N_{3S} of BO_{3S}, and the fraction N_{3A} of BO_{3A} on R and K values is much more interesting and valuable. The experimental values of $N_4(E)$, $N_{3S}(E)$ and $N_{3A}(E)$ of different R for each of the five families of glass samples are shown in figure 15, figure 16 and figure 17. Also, fractions of $N_4(C)$, $N_{3S}(C)$ and $N_{3A}(C)$ for each of five family glasses predicted by the structural model are plotted as a function of R in these figures. The experimental values of $N_4(E)$, $N_{3S}(E)$ and $N_{3A}(E)$ are in reasonably good agreement with the values $N_4(C)$, $N_{3S}(C)$ and $N_{3A}(C)$ predicted by the structural model, within

experimental error. This result supports the structural model proposed by this paper.

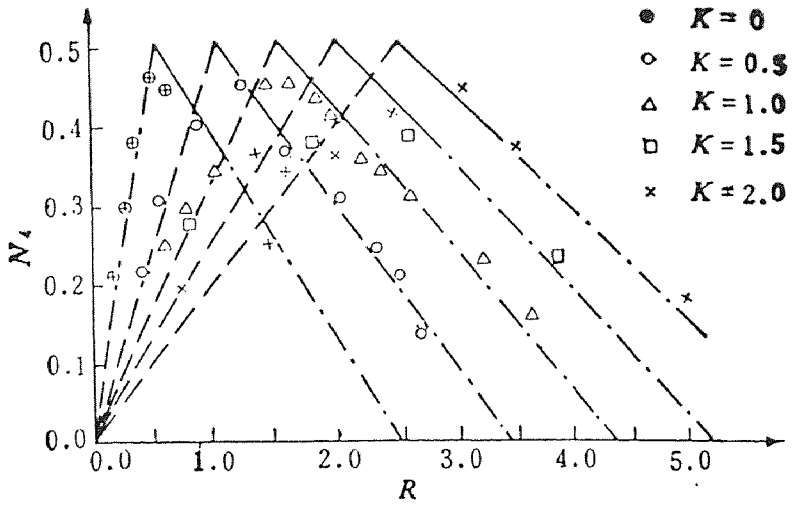

Figure 15 N_4 versus R for $xNa_2O{\cdot}yB_2O_3{\cdot}zV_2O_5$ glasses.

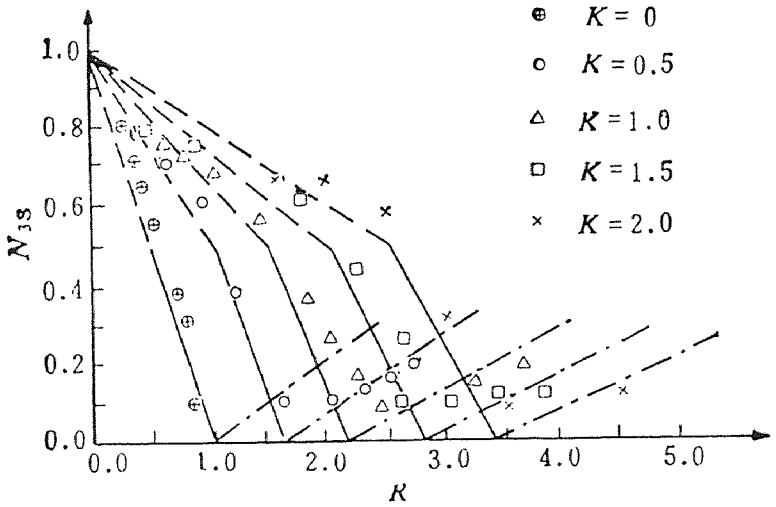

Figure 16 N_{3S} versus R for $xNa_2O{\cdot}yB_2O_3{\cdot}zV_2O_5$ glasses.

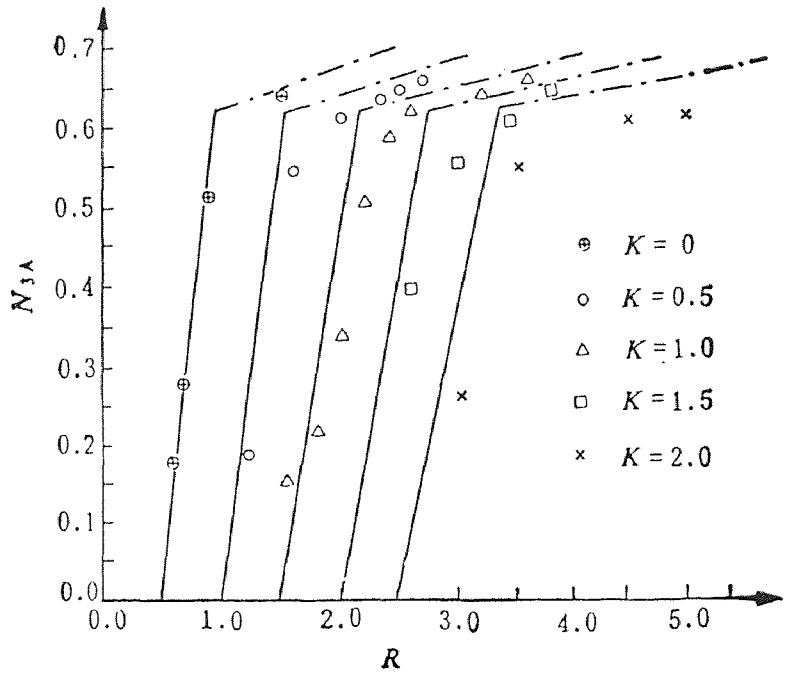

Figure 17 N_{3A} versus R for $xNa_2O{\cdot}yB_2O_3{\cdot}zV_2O_5$ glasses.

By analyzing the behavior of the dependence of N_4, N_{3S} and N_{3A} on R, the spanning range of R for each K family glass can be resonably divided into three regions in figure 15, figure 16 and figure 17.

In the first region, $R \leq 0.5+K$, $N_4(C)$, $N_{3S}(C)$ versus R are represented by dashed line. By inscreasing R, figure 15 and figure 16 show that the values of N_4 increase while the values of N_{3S} decrease. When $R = 0.5+K$, values of N_4 reach their maximum values, and values of N_{3S} reach their first critical turning points. Values of N_{3A} do not appear in the first region.

In the second region, $0.5+K \leq R \leq 1.0+1.2K$, $N_4(C)$, $N_{3S}(C)$ and $N_{3A}(C)$ versus R are represented by solid line. By increasing R, figure 15, figure 16 and figure 17 show that the values of N_4 and N_{3S} decrease while the values of N_{3A} increase. When $R = 1.0+1.2K$, values of N_{3S} reach their minimum values (approximately, zero values) and values of N_{3A} reach their first critical turning points.

In the third region, $R \geq 1.0+1.2K$, $N_4(C)$, $N_{3S}(C)$ and $N_{3A}(C)$ are represented by dash-dotted line. By increasing R, figure 15, figure 16 and figure 17 show that the values of N_4 decrease at the same rate as they do in the second region while the values of N_{3S} and N_{3A} increase.

5.3.2 Structure Model of Sodium Borovanadate Glass and Discussion

Binary alkali borate glasses have been studied by many authors [7,8,9,12] by means of ^{11}B NMR , Infrared and Raman Spectroscopies. Krough-Moe [9], Y. H.Yun and P. J. Bray [7] state that alkali borate glasses for all different compositions (different R values) are constructed as a random network of nine basic structural groups which occur in crystalline compounds. These structural groups are shown in figure 18 [9,7,10]. All the grouping units are formed from different compositions of alkali oxide reacted with boron oxide (boroxol units).

For binary sodium borate glasses $xNa_2O{\cdot}yB_2O_3$, Krough-Moe's [9] structural model concluded that

(a) Pure boron oxide glass consists mainly of boroxol units. In the region $0 \leq R \leq 0.25$ ($R=mol\%Na_2O/mol\%B_2O_3$), the addition of one molecule of Na_2O results in the formation of one tetraborate unit at the expense of four boroxol units.

(b) When $R = 0.25$, the glass consists mainly of tetraborate units. In the region $0.25 \leq R \leq 0.5$, the addition of one molecule of Na_2O results in the formation of two diborate units at the expense of one tetraborate unit.

(c) When $R = 0.5$, the glass consists mainly of diborate units.

Yun and Bray [7] proposed the further structural model of binary sodium borate glasses for region $R \geq 0.5$, that is

(d) For $0.5 \leq R \leq 1$, the addition of one molecule of Na_2O results in the formation of 2.5 metaborate units and 1.5 loose BO_4 units at the expense of one diborate unit.

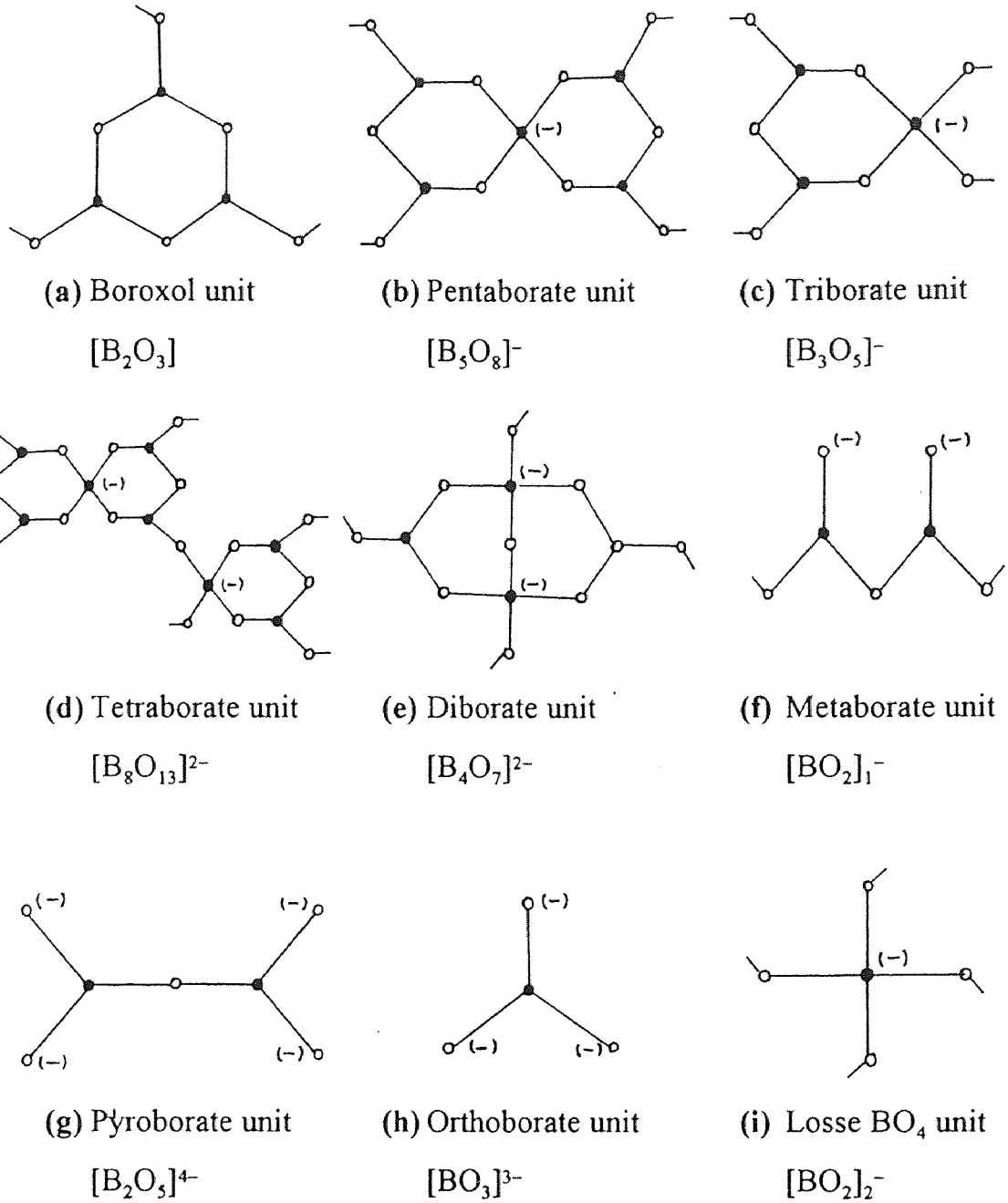

Figure 18 The nine basic structural groups in alkali borate glasses.

(e) When R = 1, the glass consists mainly of metaborate units and loose BO_4 units. For R≥1, the addition of one molecule of Na_2O results in the formation of

0.6 pyroborate units and 0.4 orthoborate units at the expense of 1.1 metaborate units and 0.5 loose BO_4 units. The upper limit on R is at about R = 1.86.

The experimental values of N_4, N_{3S} and N_{3A} of ^{11}B NMR for binary sodium borate glasses are in reasonably good agreement with the values predicted by the above structural model.

The binary lithium vanadate $xLi_2O \cdot zV_2O_5$ glasses have been studied and described in several reports [11]. There is a majority agreement as to the existence of LiV_3O_8, $LiVO_3$ and Li_3VO_4. Extensive glass formation was observed from pure V_2O_5 (R=mol%Li_2O/mol%V_2O_5=0) to higher Li_2O content at about R=0.6/0.4=1.5.

In the region about $0 \leq R \leq 1/3$, the main reaction occuring in glass is that the addition of Li_2O results in the formation of LiV_3O_8 at the expense of V_2O_5.

When R = 1/3, the glass consists mainly of LiV_3O_8. In the region about $1/3 \leq R \leq 1$, the main reaction occuring in glass is that the addition of Li_2O results in the formation of $LiVO_3$ at the expense of LiV_3O_8.

When R = 1, the glass consists mainly of $LiVO_3$. In the region about $1 \leq R \leq 1.5$, the main reaction happened in glass is that the addition of Li_2O results in the formation of Li_3VO_4 at the expense of $LiVO_3$.

Now, studies are focused on the ternary sodium borovanadate glasses. By inspecting figure 15, figure 16 and figure 17, it is observed that the changing trend of experimental values of $N_4(E)$, $N_{3S}(E)$ and $N_{3A}(E)$ versus R for the ternary $xNa_2O \cdot yB_2O_3 \cdot zV_2O_5$ glasses is similar to that for the binary $xNa_2O \cdot yB_2O_3$ glasses. But, the decreasing rate or increasing rate of values of the former is slower than that of the latter, because the added V_2O_5 shares the Na_2O with B_2O_3. This characteristic implies that this ternary $xNa_2O \cdot yB_2O_3 \cdot zV_2O_5$ can be studied somewhat like a binary sodium borate glass with the consideration about the sharing of Na_2O by both B_2O_3 and V_2O_5. According to the studies of the binary

sodium borate glasses, the binary alkali vanadate glasses, and the behaviors of figure 15, figure 16 and figure 17, the structural model for the ternary sodium borovanadate can be proposed as follows:

When x molecules of Na_2O are added into glasses, x_1 molecules of Na_2O react with boron oxide or borate glasses and x_2 molecules of Na_2O react with vanadium oxide or vanadate glasses. It can be concluded by inspecting figure 15, figure 16 and figure 17 that the ratio of x_1 to x_2 is proportional to K (K=z/y), that is,

$$\frac{x_1}{x_2}=C\cdot K$$

where C is the proportional constant which can be determined experimentally from the relationship of $N_4(E) \sim R$, $N_{3S}(E) \sim R$ and $N_{3A}(E) \sim R$.

For $R \leq 0.5+K$, $C=2$.

For $0.5+K \leq R \leq 1+1.2K$, $C=0.4$.

For $R \geq 1+1.2K$, $C=0.4$

The reaction structural model is proposed as following:

1). In the first region, $R \leq 0.5+K$, there are three reaction processes and this region can be further divided into three subregions which are, $0 \leq R \leq \frac{1}{6}+\frac{K}{3}$, $\frac{1}{6}+\frac{K}{3} \leq R \leq \frac{1}{4}+\frac{K}{2}$, and $\frac{1}{4}+\frac{K}{2} \leq R \leq \frac{1}{2}+K$.

a). For $0 \leq R \leq \frac{1}{6}+\frac{K}{3}$, of the one molecule of additional Na_2O, $\frac{1}{2K+1}$ molecules of Na_2O destroy $\frac{4}{2K+1}$ molecules of B_2O_3 to form $\frac{1}{2K+1}$ tetraborate

units, and $\frac{2K}{2K+1}$ molecules of Na_2O destroy $\frac{6K}{2K+1}$ molecules of V_2O_5 to form $\frac{4K}{2K+1}$ molecules of NaV_3O_8. In equation form, the reaction model is

$$\frac{1}{2K+1}Na_2O + \frac{4}{2K+1}B_2O_3 + \frac{2K}{2K+1}Na_2O + \frac{6K}{2K+1}V_2O_5 \rightarrow$$

$$\frac{1}{2K+1}([B_8O_{13}]^{2-} + 2Na^+) + \frac{4K}{2K+1}NaV_3O_8 \qquad (25)$$

where $[B_8O_{13}]^{2-}$ denotes a tetraborate unit. Let (B_4), (B_{3S}), and (B_{3A}) express the amount of boron atoms in four-coordination with oxygen $[BO_4]$, the amount of boron atoms in symmetric three-coordination with oxygen $[BO_{3S}]$, and the amount of boron atoms in asymmetric three-coordination with oxygen $[BO_{3A}]$, respectively. Equation (25) reaction model predict that, for one additional Na_2O molecule, (B_4) increases by $\frac{2}{2K+1}$, (B_{3S}) decreases by $\frac{2}{2K+1}$, and (B_{3A}) remains zero, that is, $(B_4) = \frac{2}{2K+1}x$, $(B_{3S}) = (B) - \frac{2}{2K+1}x$, and $(B_{3S}) = 0$. So, the reaction model predicts that

$$N_4 = \frac{(B_4)}{(B)} = \frac{\frac{2}{2K+1}x}{2y} = \frac{R}{2K+1} \qquad (26)$$

$$N_{3S} = \frac{(B_{3S})}{(B)} = \frac{2y - \frac{2}{2K+1}x}{2y} = 1 - \frac{R}{2K+1} \qquad (27)$$

$$N_{3A} = \frac{(B_{3A})}{(B)} = 0 \qquad (28)$$

When $R = \frac{1}{6}+\frac{K}{3}$, all z moleculecules of V_2O_5 are destroyed to form $\frac{2z}{3}$ molecules of NaV_3O_8, and $\frac{2y}{3}$ molecules of B_2O_3 are destroyed to form $\frac{y}{6}$ tetraborate units. The glass system mainly consists of $\frac{y}{3}B_2O_3$, $\frac{y}{6}([B_8O_{13}]^{2-} + 2Na^{+})$, $\frac{2z}{3}NaV_3O_8$.

b). For $\frac{1}{6}+\frac{K}{3} \le R \le \frac{1}{4}+\frac{K}{2}$, of the one molecule of additional Na_2O, $\frac{1}{2K+1}$ molecules of Na_2O destroy $\frac{4}{2K+1}$ molecules of B_2O_3 to form $\frac{1}{2K+1}$ tetraborate units, and $\frac{2K}{2K+1}$ molecules of Na_2O destroy $\frac{2K}{2K+1}$ molecules of NaV_3O_8 to form $\frac{6K}{2K+1}$ molecules of $NaVO_3$. In equation form, the reaction model is

$$\frac{1}{2K+1}Na_2O + \frac{4}{2K+1}B_2O_3 + \frac{2K}{2K+1}Na_2O + \frac{2K}{2K+1}NaV_3O_8 \rightarrow$$

$$\frac{1}{2K+1}([B_8O_{13}]^{2-} + 2Na^{+}) + \frac{6K}{2K+1}NaVO_3 \qquad (29)$$

This reaction model still predicts that

$$N_4 = \frac{R}{2K+1} \qquad (26)$$

$$N_{3S} = 1 - \frac{R}{2K+1} \qquad (27)$$

$$N_{3A} = 0 \qquad (28)$$

When $R = \frac{1}{4}+\frac{K}{2}$, all y molecules of B_2O_3 are destroted to form $\frac{y}{4}$ tetraborate units, $\frac{z}{6}$molecules of NaV_3O_8 are destroyed to form $\frac{z}{2}$ molecules of $NaVO_3$, and $\frac{z}{2}$

molecules of NaV_3O_8 remain unreacted. The glass system mainly consists of $\frac{y}{4}([B_8O_{13}]^{2-} + 2Na^+)$, $\frac{z}{2}NaVO_3$, $\frac{z}{2}NaV_3O_8$.

c). For $\frac{1}{4}+\frac{K}{2} \le R \le \frac{1}{2}+K$, of the one molecule of additional Na_2O, $\frac{1}{2K+1}$ molecules of Na_2O destroy $\frac{1}{2K+1}$ tetraborate units to form $\frac{2}{2K+1}$ diborate units, and $\frac{2K}{2K+1}$ molecules of Na_2O destroy $\frac{2K}{2K+1}$ molecules of NaV_3O_8 to form $\frac{6K}{2K+1}$ molecules of $NaVO_3$. In equation form, the reaction model is

$$\frac{1}{2K+1}Na_2O + \frac{1}{2K+1}([B_8O_{13}]^{2-} + 2Na^+) + \frac{2K}{2K+1}Na_2O +$$

$$\frac{2K}{2K+1}NaV_3O_8 \rightarrow \frac{2}{2K+1}([B_4O_7]^{2-} + 2Na^+]) + \frac{6K}{2K+1}NaVO_3 \qquad (30)$$

This reaction model still predicts that

$$N_4 = \frac{R}{2K+1} \qquad (26)$$

$$N_{3S} = 1 - \frac{R}{2K+1} \qquad (27)$$

$$N_{3A} = 0 \qquad (28)$$

When $R = \frac{1}{2}+K$, all tetraborate units are destroyed to form $\frac{y}{2}$ diborate units, and all NaV_3O_8 are destroyed to form 2z molecules of $NaVO_3$. The glass system mainly consists of $\frac{y}{2}([B_4O_7]^{2-} + 2Na^+)$, $2z\ NaVO_3$.

2). In the second region, $0.5 + K \leq R \leq 1+1.2K$, of the one molecule of additional Na_2O, $\frac{1}{1+0.4K}$ molecules of Na_2O destroy $\frac{1}{1+0.4K}$ diborate units to form $\frac{2.5}{1+0.4K}$ metaborate units and $\frac{1.5}{1+0.4K}$ loose BO_4 units, and $\frac{0.4K}{1+0.4K}$ molecules of Na_2O destroy $\frac{0.4K}{1+0.4K}$ molecules of $NaVO_3$ to form $\frac{0.4K}{1+0.4K}$ molecules of Na_3VO_4. In equation form, the reaction model is

$$\frac{1}{1+0.4K}Na_2O+\frac{1}{1+0.4K}([B_4O_7]^{2-} + 2Na^+)+\frac{0.4K}{1+0.4K}Na_2O+\frac{0.4K}{1+0.4K}NaVO_3 \rightarrow$$

$$\frac{2.5}{1+0.4K}([BO_2]_1^-+Na^+)+\frac{1.5}{1+0.4K}([BO_2]_2^-+Na^+)+\frac{0.4K}{1+0.4K}Na_3VO_4 \qquad (31)$$

where $[BO_2]_1^-$ and $[BO_2]_2^-$ denote metaborate unit and loose BO_4 unit, respectively. This reaction model predicts that

$$N_4 = \frac{25+18K}{40+16K} - \frac{5}{20+8K}R \qquad (32)$$

$$N_{3S} = \frac{5+6K}{5+2K} - \frac{5}{5+2K}R \qquad (33)$$

$$N_{3A} = -\frac{25+50K}{40+16K} + \frac{25}{20+8K}R \qquad (34)$$

When $R = 1+1.2K$, all diborate units are destroyed to form 1.25y metaborate units and 0.75y loose BO_4 units, 0.2z molecules of $NaVO_3$ are destroyed to form 0.2z molecules of Na_3VO_4, and 1.8z molecules of $NaVO_3$ remain unreacted. The glass system mainly consists of 1.25y($[BO_2]_1^-+Na^+$), 0.75y($[BO_2]_2^-+Na^+$), 0.2z Na_3VO_4, 1.8z $NaVO_3$.

3) In the third region, $R \geq 1+1.2K$, of the one molecule of additional Na_2O, $\frac{1}{1+0.4K}$ molecules of Na_2O destroy $\frac{1.1K}{1+0.4K}$ metaborate units and $\frac{0.5}{1+0.4K}$ loose

BO_4 units to form $\frac{0.6}{1+0.4K}$ pyroborate units and $\frac{0.4}{1+0.4K}$ orthoborate units, $\frac{0.4K}{1+0.4K}$ molecules of Na_2O destroy $\frac{0.4K}{1+0.4K}$ molecules of $NaVO_3$ to form $\frac{0.4K}{1+0.4K}$ molecules of Na_3VO_4. In equation form, the reaction model is

$$\frac{1}{1+0.4K}Na_2O+\frac{1.1K}{1+0.4K}([BO_2]_1^-+Na^+)+\frac{0.5}{1+0.4K}([BO_2]_2^-+Na^+)$$

$$+\frac{0.4K}{1+0.4K}Na_2O+\frac{0.4K}{1+0.4K}NaVO_3 \longrightarrow \frac{0.6}{1+0.4K}([B_2O_5]^{4-}+4Na^+)$$

$$+\frac{0.4}{1+0.4K}([BO_3]^{3-}+3Na^+)+\frac{0.4}{1+0.4K}Na_3VO_4 \qquad (35)$$

where $([B_2O_5]^{4-}+4Na^+]$ and $([BO_3]^{3-}+3Na^+)$ denote pyroborate unit and orthoborate unit, respectively. This reaction model predicts that

$$N_4 = \frac{25+18K}{40+16K} - \frac{5}{20+8K}R \qquad (36)$$

$$N_{3S} = -\frac{5+6K}{25+10K} + \frac{1}{5+2K}R \qquad (37)$$

$$N_{3A} = \frac{115+38K}{200+80K} + \frac{1}{20+8K}R \qquad (38)$$

Using equations (26), (27), (28), (32), (33), (34), (36), (37) and (38) with values of K=0, 0.5, 1.0, 1.5 and 2.0, the curves of N_4 ~ R, N_{3S} ~ R and N_{3A} ~ R of each K value family for the proposed reaction model are plotted in figure 15, figure 16 and figure 17. Also, all the $N_4(C)$, $N_{3S}(C)$ and $N_{3A}(C)$ values are listed in table 5. Figure 15, figure 16, figure 17 and table 5 show that the theoretical model values of $N_4(C)$, $N_{3S}(C)$ and $N_{3A}(C)$ are in reasonablly good agreement with the experimental values of $N_4(E)$, $N_{3S}(E)$ and $N_{3A}(E)$, which are obtained by ^{11}B NMR computer simulation techniques.

CHAPTER 6

CONCLUSION

A computer program is devised which can calculate the powder pattern for arbitrary quadrupolar and chemical shift parameters, convolute it with an appropriate Gaussian function that simulates the effects of dipolar broadening, and ultimately form a derivative-like spectrum which is characteristic of the experimental results. The development of this program which simulates the NMR spectra observed in powdered and glassy samples makes it possible to calculate the relevant Hamiltonian parameters for a NMR spectrum occuring in a powdered solid sample. Table 3 in section 5.2 shows the values of the relative parameters (Q_{cc}, η, σ) of the three distinct boron sites in the system of $xLi_2O{\cdot}yB_2O_3{\cdot}zV_2O_5$ glasses by using computer simulation method. In addition, this computer technique can also be used to calculate the relative intensities of several overlapping spectra. Table 5 in section 5.3 shows the results of the relative intensities (N_4, N_{3S}, N_{3A}) of overlapping spectra due to three different boron-oxygen network units BO_4, BO_{3S}, and BO_{3A}.

Typical theoretical behavior of the powder pattern for the central transition in the presence of both quadrupolar and chemical shift interactions is discussed in chapter 2. The locations of shoulders and singularities of the powder patterns are listed in table 1 and table 2 in chapter 2.

The "noise" of the simulated-spectrum caused by numerical calculation is analyzed in section 5.1. Figure 8a and figure 8b indicate that the smaller the division of the $\cos\theta-\phi$ space into uniform grids, the less the "noise", and consequently, the greater the signal to noise ratio for the powder pattern.

The details of the simulation procedure are discussed in section 5.2. It is noted that chemical shift effects are negligible at low frequencies, so that the quadrupole parameters, Q_{cc}, η, and the dipolar width 2σ, can easily be estimated from the experimental spectra taken at lower frequency. second, the experimental spectra taken at the higher available frequency are fitted by varying the three chemical shift parameters (σ_1, σ_2, σ_3) of the calculated-spectra, and finally, minor corrections for all of the parameters results in computed spectra which are in agreement with the experimental spectra at all frequencies.

The computer simulation techniques are applied to the studies of ^{11}B NMR spectra of the sodium borovanadate glass system and the data of $N_4(E)$, $N_{3S}(E)$ and $N_{3A}(E)$ as functions of R and K are obtained. The relative abundance of each of different borate units (networks) in the glass system are obtained when the compositions (R, K) of the glass system are varied, as shown in figures 15, 16 and 17. Considering figures 15, 16 and 17, together with the studies of some binary glass systems of alkali borates and lithium vanadates by the other authors [7, 9, 11], the structural reaction model for the ternary sodium boro-vanadate glass system as proposed in section 5.3 is expressed by the equations (25), (29), (30), (31) and (35). According to this structural reaction model, the data of $N_4(C)$, $N_{3S}(C)$ and $N_{3A}(C)$ as functions of R and K are calculated, and the results are in reasonable agreement with the experimental data of $N_4(E)$, $N_{3S}(E)$ and $N_{3A}(E)$ which are obtained by using our computer simulation method.

REFERENCES

[1] Abragam., A. 1961. *The Principle of Nuclear Magnetism.* London: Oxford University Press.

[2] Slichter, C. P. 1963. *Principle of Magnetic Resonance.* New York: Harper and Row Publishes, Inc.

[3] Baugner, J. F., P. C. Taylor, T. Oja and P. J. Bray. 1969. "Nuclear Magnetic Resonance Powder Patterns in the Presence of Completely Asymmetric Quadrupole and Chemical Shift Effects: Application to Metavanadates." J.Chem.Phys. 50: 4914–4925.

[4] Narita, K., J. Umeda, and H. Kusumoto. 1966. "Nuclear Magnetic Resonance Powder Patterns of the Second-Order Nuclear Quadrupole Interaction in Solids with Asymmetric Field Gradient." J. Chem. Phys. 44(7): 2721–2723.

[5] Kaplan, W. 1952. *Advanced Calculus.* Mass.: Addison–Wesley Publ. Co., Inc., Reading.

[6] Mehring, M. 1983. *Principle of High Resolution NMR in Solids.* Berlin: Verlag–Springer Press.

[7] Yun, Y. H., and P. J. Bray. 1981. "^{11}B Nuclear Magnetic Resonance Studies of Li_2O–B_2O_3 Glasses of High Li_2O Cotent." J. Non-cryst. Solid. 44:227–237.

[8] Zachariasen, W. H. 1932. "The Atomic Arrangement in Glass." J. Amer. Chem. 54: 3841–3851.

[9] Krogh-Moe, J. 1965. "Interpretation of the Infra-red Spectra of Boron Oxide and Alkali Borate Glasses." Phys. Chem. Glasses. 6: 46–54.

[10] Yun, Y. H. and P. J. Bray. 1978. "Nuclear Magnetic Resonance Studies of the Glasses in the System Na_2O–B_2O_3–SiO_2." J. Non-Cryst. Solids. 27: 363–380.

[11] Nassau, K. and D. W. Murphy. 1981. "The Quenching and Electrochemical Behavior of $Li_2O–V_2O_5$ Glasses." J. Non-Cryst. Solids. 44: 297–304.

[12] Greenblatt, S. and P. J. Bray. 1967. "A Discussion of the Fraction of Four-Co-ordinated Boron Atoms Presence in Borate Glasses." Phys. Chem. Glasses. 8: 213–217.